



HAL
open science

Addressing the issues of non-isotropy and non-additivity in the development of quantum chemistry-grounded polarizable molecular mechanics.

Nohad Gresh, Krystel El Hage, Elodie Goldwaser, Benoit De Courcy, Robin Chaudret, David Perahia, Christophe Narth, Louis Lagardere, Filippo Lipparini, Jean-Philip Piquemal

► To cite this version:

Nohad Gresh, Krystel El Hage, Elodie Goldwaser, Benoit De Courcy, Robin Chaudret, et al.. Addressing the issues of non-isotropy and non-additivity in the development of quantum chemistry-grounded polarizable molecular mechanics.. J. L. Rivail, M. Ruiz-Lopez, X. Assfeld. Quantum Modeling of Complex Molecular Systems, 21, Springer, pp.1-49, 2015, 10.1007/978-3-319-21626-3_1 . hal-01104542

HAL Id: hal-01104542

<https://hal.science/hal-01104542v1>

Submitted on 19 Jan 2015

HAL is a multi-disciplinary open access archive for the deposit and dissemination of scientific research documents, whether they are published or not. The documents may come from teaching and research institutions in France or abroad, or from public or private research centers.

L'archive ouverte pluridisciplinaire **HAL**, est destinée au dépôt et à la diffusion de documents scientifiques de niveau recherche, publiés ou non, émanant des établissements d'enseignement et de recherche français ou étrangers, des laboratoires publics ou privés.

Addressing the issues of non-isotropy and non-additivity in the development of quantum chemistry-grounded polarizable molecular mechanics.

Nohad Gresh^{1,2*}, Krystal El Hage^{1,3}, Elodie Goldwaser^{1,2}, Benoit de Courcy^{1,2}, Robin Chaudret², David Perahia⁴, Christophe Narth², Louis Lagardere,² Filippo Lipparini,² Jean-Philip Piquemal^{2*}

¹Chemistry and Biology, Nucleo(s)tides and Immunology for Therapy (CBNIT), UMR 8601 CNRS, UFR Biomédicale, Paris, France

²Laboratoire de Chimie Théorique, Sorbonne Universités, UPMC, UMR7616 CNRS, Paris, France

³Centre d'Analyses et de Recherche, UR EGFEM, Faculté des Sciences, Saint Joseph University of Beirut, Beirut 1107 2050, Lebanon

⁴Laboratoire de Biologie et de Pharmacologie Appliquées (LPBA), UMR 8113 CNRS, Ecole Normale Supérieure de Cachan,

to appear in Quantum Modeling of Complex Molecular Systems, Editors: J. L. Rivail, M. Ruiz-Lopez and X. Assfeld, Springer.

Summary. We review two essential features of the intermolecular interaction energies (ΔE) computed in the context of quantum chemistry (QC): non-isotropy and non-additivity. Energy-decomposition analyses show the extent to which each comes into play in the separate ΔE contributions, namely electrostatic, short-range repulsion, polarization, charge-transfer and dispersion. Such contributions have their counterparts in anisotropic, polarizable molecular mechanics (APMM), and each of these should display the same features as in QC. We review examples to evaluate the performances of APMM in this respect. They bear on the complexes of one or several ligands with metal cations, and on multiply H-bonded complexes. We also comment on the involvement of polarization, a key contributor to non-additivity, in the issues of multipole transferability and conjugation. In the last section we provide recent examples of APMM validations by QC, which relate to interactions taking place in the recognition sites of kinases and metalloproteins. We conclude by mentioning prospects of extensive applications of APMM.

Introduction. The field of molecular simulation is undergoing major strides forward. It is spearheaded by ab initio quantum chemistry (QC), whose realm of applications is being extended to complexes of increasing size, nowadays totaling a few hundreds of atoms, and are amenable as well to increasingly long simulation times as is the case for Car-Parrinello (CP) [1] or Born-Oppenheimer (BO) [2] molecular dynamics (MD) approaches. Such extensions are enabled by advances both in informatics and in the QC codes themselves. The first kind of advances results from progress both in computer hardware, as exemplified by the advent of Graphics Processor Units (GPU) [3] and in computer software, as enabled by parallelism on Open MP/MPI software [4]. The second advances are due to promising developments in linear-scaling and divide-and-conquer approaches [5]. Despite such advances, simulations of very large molecular complexes and/or on very long-time scale MD or of computer-intensive Monte-Carlo (MC) simulations are likely to remain out of reach of high-level QC for a long foreseeable time in a diversity of domains. These encompass drug design, protein folding, or material science. An appealing alternative consists into the so-called QM/MM (Quantum mechanics/molecular mechanics) approaches, in which the core of the recognition site is treated quantum-mechanically while the periphery is treated by classical MM. Multiscale approaches are a generalization of QM/MM [6]. However, such approaches could not be used in the absence of a single 'privileged' recognition site, as is the case for multidomain sites in, eg, protein-nucleic acid (NA), protein-protein or NA-NA recognition. There are also examples of enlarged or accessible recognition sites, such that long-range polarization effects could blur the distinction between QM and MM zones. This can occur with the complexes of inhibitors to the Zn-metalloenzyme phosphomannose isomerase, in which networks of polarizable water molecules can connect together the inhibitor in the recognition site to farther sites on N- and/or C-terminal sites [7]. 'Classical' MM/MD potentials are on the other hand fully able nowadays to handle very large molecular complexes over time-scales which even for proteins can approach the microsecond if not the millisecond time. They have rendered prominent service to the field and will most probably continue to do so for a long-time to come. Nevertheless their limitations are duly recognized, notably the absence of non-additivity and the lack of appropriate directionality. Such shortcomings will not be commented in this review. An ideal situation would consist into a QC-grounded MM potential formulated and calibrated so as to reproduce each individual QC contribution. Transferability can be compromised if the aim of a given MM potential were limited to reproduce the total QC intermolecular interaction, $\Delta E(\text{QC})$ forfeiting that on its individual contributions. It is also clear that a term-to-term agreement with the $\Delta E(\text{QC})$ contributions should carry out beyond

the training set used in the calibration. Striving at reproducing QC results has been the object of several endeavors, past and present. These have been surveyed in several recent reviews [8]. Summarizing, we recall that the main efforts bore on the inclusion of polarization: dipole polarization [8], charge equalization [9], or Drude models [10]. It is fitting to recall that the very first inclusion of polarization for the modeling of biological molecules were from the mid- sixties [11] and mid-seventies [6a]. A subset of 'polarizable' MM/MD potentials have also targeted first-order electrostatics, resorting to distributed multipoles derived from ab QC calculations on the fragments [12-17]. This is the case of the SIBFA (Sum of Interactions Between Fragments Ab initio computed [12] procedure, on which this review focuses, and which was among the prime ones in this regard. Further refinements have also borne on the two short-range contributions, repulsion in first-order and charge-transfer in second-order. This appears to restrict the subset of polarizable potentials to SIBFA, ORIENT [13], and the Effective Fragment Potential (EFP) [14].

This review is organized as follows. We use here italics to underline the sought-for features. We will first summarize the features of the SIBFA potential, in light of the requirements for *transferability*. We will then present the results of validation tests regarding first *anisotropy*, then *non-additivity*. Their synergistic impact will be illustrated with the complexes of halobenzene derivatives with a guanine-cytosine base-pair in the recognition site of the HIV-1 nucleocapsid. This will be extended to a case problem in which both come into play and should enable to address in synergy two additional issues, namely *multipole transferability* and *conjugation*. We will next present results from recent studies from two of our Laboratories. The first study relates to the organization of highly structured waters in a bimetallic Zn/Cu enzyme, superoxide dismutase (SOD). The two other relate to inhibitor or ligand binding to a tyrosine kinase, Focal Adhesion Kinase (FAK), on the one hand, and to a Zn-metalloenzyme, phosphomannose isomerase (PMI) on the other hand. These will help to highlight the importance of the second-order contributions, and possibly non-additivity, on molecular recognition.

Procedure.

In the SIBFA procedure, the total intermolecular interaction energy between molecules or molecular fragments is computed as a sum of five contributions:

$$\Delta E_{\text{tot}} = E_{\text{MTP}} + E_{\text{rep}} + E_{\text{pol}} + E_{\text{ct}} + E_{\text{disp}}$$

which are the electrostatic multipolar, the short-range repulsion, the polarization, the charge-transfer, and the dispersion contributions.

E_{MTP} is computed as a sum of multipole-multipole interactions, encompassing six terms from monopole-monopole till quadrupole-quadrupole. The multipoles are located on the atoms and mid-points of the chemical bonds, and are derived from the ab initio QC molecular orbitals (MO) of the fragment. We resort to a procedure pioneered in 1970 by Claverie, Dreyfus and Pullman (CDP) at the Institut de Biologie Physico-Chimique in Paris [18]. It was initially applied to computations of the Molecular Electrostatic Potential (MEP) around biologically important molecules, such as the nucleic acid bases [19], DNA and RNA [20], proteins [21], phospholipids [22] and ionophores [23]. The CDP method was first applied to the computations of intermolecular interaction energies in 1979 in the context of a polarizable potential [24] and, in 1980-1983, for a series of molecular recognition problems [25] using forerunners of the SIBFA procedure. Current applications have since resorted to a variant of the CDP procedure due to Vigné-Maeder and Claverie [26]. For completeness we mention that the derivation of distributed multipoles was also done in the context of IEHT wavefunctions by Rein in 1973 [27], and, regarding ab initio QC MO's, in the early eighties by Stone et al. [28], Sokalski et al. [29], and Karlstrom et al. [30]. The more recent OPEP procedure enables to derive both distributed multipoles and polarizabilities from such MO's [31].

Subsequent improvements to E_{MTP} have consisted into including an explicit 'penetration' term, E_{pen} . This is an overlap-dependent term: it translates the fact that at short intermolecular distances, there is a lesser shielding of the nuclear charge of a given atom by its own electronic density, due to its 'penetration' by the corresponding density of the incoming atom, and conversely. This results into an actual increase of the electron-nucleus attraction of the interacting pair. The first formulations of E_{pen} were in 2000-2001 in the context of EFP [32] and in 2003 in the context of SIBFA [33]. The latter has been used systematically ever since 2005 with this procedure. Other formulations have also been recently put forth [34]. The formulation by Piquemal et al. recently underwent a promising extension enabling to use it in conjunction with the Particle Mesh Ewald (PME) procedure [Narth et al., submitted]. This

will pave the way for efficient MD simulations on very large systems in the context of the SIBFA or AMOEBA procedures.

The other contribution of predominantly electrostatic nature is polarization. It translates the gain in energy upon rearrangement of the electronic distribution of a given molecular fragment due to the electrostatic field generated on it by all the other interacting fragments. E_{pol} on any 'polarizable' center is a function of the electrostatic field it undergoes and of its polarizability. The field is computed with the same distributed multipoles as E_{MTP} and is screened by a Gaussian function, S , of the distance between the center and the interacting polarizing partner, modulated by the mean of the effective radii of the interacting pair. The polarizability can be used: -either as a scalar, the magnitude of which is derived from experimental measurements. This was done in the earlier versions of SIBFA and in most contemporary polarizable potentials which use the induced dipole approach [8]; -or as a QC-derived tensor. This is the case of but a handful of polarizable potentials, namely EFP, SIBFA, and ORIENT. In fact, both SIBFA and EFP resort to the same procedure to derive the polarizabilities, specifically a method published in 1989 by Garmer and Stevens (GS) [35], locating them on the centroids of the Boys localized molecular orbitals (LMO): these are the barycenters of the chemical bonds and the 'tips' of the saturated lone pairs. The two first papers reporting the use of the GS polarizabilities, namely using EFP and SIBFA, were actually published in the same 1994 issue of the ACS Symposium series [36].

Thus given any rigid molecule or molecular fragment, we derive once and for all, in a consistent fashion both distributed multipoles and polarizabilities. These are stored in the SIBFA library as one file, along with the information on the internal geometry and connectivities and types of atoms. Each fragment-specific file can be extracted and concatenated with others whenever the fragment is needed to assemble a large, flexible molecule, or a biomolecule, such as a protein or a nucleic acid.

SIBFA embodies two overlap-dependent contributions.

E_{rep} in first-order is formulated under the form of a sum of bond-bond, bond-lone pair, and lone pair-lone pair interactions. This was inspired by an earlier proposal by Murrell et al. [37] following which the exchange-repulsion is proportional to the square of the intermolecular overlap between localized orbitals. For each pair of interacting orbitals, it could be formulated as S^2/R^n , S denoting their overlap and R the distance between their centroids, n taking the

values of 1, 2 and possibly beyond. In the context of SIBFA, representations of the orbitals are the chemical bonds and the lone-pairs.

The formulation of E_{ct} in second order is based on another work by Murrell et al. [38], in which it is formulated as the integral of an overlap transition density convoluted with the electrostatic potential it undergoes. Starting from it, E_{ct} was derived as a function of the overlap between representations of the localized orbitals of the electron-donor fragment and of the virtual orbitals of the electron-acceptor fragment [39]. On account of their greater mutual proximities, they are restricted to the sole lone-pairs of the donor, and to the sole B-H bonds of the acceptor, where B denotes any heavy atom. The different contributions are calculated for all pairs of such orbitals, and embody dependencies upon the electrostatic potentials V separately undergone by the electron-donor and by the electron acceptor in the large molecular complex. These potentials also intervene in the denominator of E_{ct} . In it the ionization potential, I , of the electron donor is modulated by the (predominantly positive) potential it undergoes; while the electron affinity of the electron acceptor, A , is modulated by the (predominantly negative) potential it undergoes. In the whole range of energy-relevant distances, this prevents the I - A differences from being negative (and therefore E_{ct} from becoming positive) whenever I has a smaller magnitude than A , as is the case for most di- or multivalent cations. We also note that those V s, along with the permanent multipoles, embody the contributions due to the induced dipoles, whence an indirect coupling between the polarization and charge-transfer contributions.

The last contribution, E_{disp} , uses a formulation by Creuzet et al [40]. It is computed as a sum of atom-atom terms with $1/R^6$, $1/R^8$, and $1/R^{10}$ dependencies. It is augmented by an explicit 'exchange-dispersion' term ($E_{exch-disp}$) and by contributions from the lone pairs at their centroid positions.

Two points could be noted at this stage. Firstly, all five SIBFA contributions, not only E_{rep} and E_{ct} , embody dependencies upon the overlap: E_{pen} for E_{MTP} ; a Gaussian screening factor of the distance between each interacting pair for E_{pol} ; and $E_{exch-disp}$ for E_{disp} . Secondly, with the exception of E_{MTP} , all contributions embody dependencies upon explicit representations of the lone pairs.

We denote throughout by ΔE the energies in the absence of E_{disp} , and by E_1 and E_2 the summed first- and second-order contributions, namely $E_1 = E_{MTP} + E_{rep}$ and $E_2 = E_{pol} + E_{ct}$, respectively.

On account of its very separability, critical for the refinement of the SIBFA potential is the availability of energy-decomposition analyses. The Reduced Variational Space (RVS) procedure by Stevens and Fink [41] was particularly instrumental. On the one hand, it affords an operational and dependable separation of E_2 into E_{pol} and E_{ct} . On the other hand, it lends itself to analyses of complexes having more than just two interacting partners. This enable to compute the separate components of E_1 and E_2 in multi-molecular complexes, evaluate the extent of their non-additivities, and how well these could be accordingly retrieved by their SIBFA counterparts. There are also other energy-decomposition analyses, such as the Constrained Space Orbital Variation (CSOV) [42] and the Symmetry-Adapted Perturbation Theory (SAPT) [43], which can both be done at the correlated level. We have resorted to the former upon dealing with open-shell cations [44] and for correlated computations [45] and are presently resorting to the latter in analyses of the interactions involving nucleic acid bases [Gresh et al., submitted].

Results and discussion.

A. Anisotropy.

MM potentials should be able to account for the fine angular features of $\Delta E(\text{QC})$ upon performing in- and out-of-plane variations of the approach of two interacting atoms at fixed equilibrium distance: that is, the departure from the assumption of atom-centered spherical symmetry. This might not be warranted by simple point-charge electrostatics and atom-atom Lennard-Jones-like formulas for E_{rep} and E_{disp} , unless neighboring atoms restricted the available space.

1) Linear water dimer. The earliest example we considered dating back from the mid-eighties is the linear water dimer at equilibrium distance ($d_{\text{OO}}=2.95 \text{ \AA}$) [39]. We monitored the evolutions, as a function of the theta angle, of $\Delta E(\text{SIBFA})$ and its E_{MTP} , E_{rep} and E_{ct} contributions (Figures 1a-c). For such evolutions the H and O atoms of the incoming OH bond of the electron-acceptor monomer predominantly sense the electrostatic potential around the O atom of the electron-donor monomer and their overlaps with its sp^3 lone-pair and there is little, if any, overlap with its two OH bonds. A very close parallelism was observed not only between the total $\Delta E(\text{SIBFA})$ and $\Delta E(\text{HF})$ energies, but also between the corresponding

individual contributions. This early demonstration already lends credence to the representation of electrostatics with QC multipoles and to that of the short-range contributions with lone-pairs. The behavior of E_{ct} was instructive. Its relative shallow behavior matching that of $E_{ct}(HF)$ was found to result from strongly opposed trends from the two sp^3 lone-pairs. The contribution from the first lone-pair increases regularly until for $\theta = 60^\circ$ the direction of the incoming HO bond aligns with it, while that of the second lone-pair decreases in concert. Past 60° , the two trends are reversed. The overall shape of ΔE appears dictated by that of E_{MTP} . This appears consistent with the proposal by Buckingham and Fowler [46]. Nevertheless the present example as well as several subsequent others (*vide infra*) clearly show instances where the other contributions do have inherently anisotropic characters of their own and do bear on the overall angular dependencies of ΔE .

2) *Cation-ligand complexes.* Zn(II) is a 'soft' divalent cation. This translates into large values of the charge-transfer and of the dispersion contributions [47], and to an enhanced propensity to bind to 'softer' ligands than oxygen, such as nitrogen and in particular sulfur. Its divalent charge gives rise to very large values of E_{MTP} and E_{pol} thus to a propensity to bind to oxygen ligands as well. In proteins and NAs, Zn binds in a versatile fashion to N, O, and S ligands, can adopt a diversity of coordination numbers ranging from 4 to 6, and can exert a structural as well as a catalytic role. It is thus most important, but it could also be particularly challenging, to correctly represent it with PMM potentials. This was addressed in 1995 [48]. By parallel QC and SIBFA computations, we probed by Zn(II) the in- and out-of-plane angularities of ΔE and its individual contributions in a diversity of complexes with N, O, and S ligands. Marked directionalities were found for both E_{rep} and E_{ct} for in-plane variations of the θ angle around the X-O-Zn bond upon binding to hydroxy (X=H), formate and formamide (X=C), and around the C-S-Zn bond of methanethiolate. These could complement or oppose the directionalities of E_{MTP} . Lesser directionalities of E_{rep} and E_{ct} were found on the other hand for out-of-plane variations on a cone at a fixed θ angle. E_{pol} was found to display a generally shallower behavior than the other contributions, although it is a major contributor to non-additivity.

3) *Hydrogen bonding to an anionic ligand.* Water acting as proton acceptor can be also used to probe the electron-rich sites of a bound ligand. An illustrative example is that of its monodentate complex with formate, upon performing in-plane variations of the C-O—H angle, at a fixed O—H distance (Figure 2). $E_{exch}(HF)$ has a marked angular character with a

maximum at 120° , which corresponds to a maximum overlap with one sp^2 oxygen lone-pair. Its behavior is paralleled by $E_{\text{rep}}(\text{SIBFA})$, while by contrast a $1/R^{12}$ atom-atom repulsion expression gives rise to a shallow behavior [49].

4) *Directionality in stacked complexes.* Stacking interactions are a major determinant of NA stability, but act also to stabilize a diversity of ordered structures. We have considered a representative stacked dimer of formamide and rotated step-wise the second monomer with respect to the first around the z-axis [49]. The curve of E_{MTP} augmented with E_{pen} is virtually superimposable over that of E_{C} (Figure 3a). The curve of E_{rep} matches well that of E_{exch} with only a small indentation at the most repulsive point (Figure 3b). The parallelism of $\Delta E(\text{SIBFA})$ with $\Delta E(\text{HF})$ is evidenced in Figure 3c. Extensions are presently underway to NA bases, and are carried out at both uncorrelated and correlated levels, and they appear conclusive as well [Gresh et al., submitted]. Such results suggest that the anisotropy of $\Delta E(\text{QC})$ in stacked complexes can be reliably accounted for in the context of the SIBFA procedure.

5) *Directionality in halobenzene complexes.* About thirty-five per cent of therapeutic drugs embody at least one halogen atom [50]. There is an outstanding feature of the CX bond in halobenzenes ($X=\text{F}, \text{Cl}, \text{Br}, \text{I}$) which was discovered thanks to quantum chemistry [51]. It is the presence of a 'sigma-hole', namely a zone of electron depletion along the bond, concomitant with a zone of electron buildup around a cone circumscribing the bond. Such features increase along the $\text{F} < \text{Cl} < \text{Br} < \text{I}$ sequence. To account for electron depletion in the context of classical MM, a fictitious charge of δ^+ has been located prolonging the CX bond, with the charge of X accordingly modified by δ^- . The magnitude of δ and the δ -X distance can be optimized in order to fit the QC-computed interaction energy of an electron-rich ligand such as water or formamide approaching the CX bond through its O atom [52]. While this representation can be successful to translate the binding of electron-rich ligands along the CX bond, it leaves the outcome unresolved regarding approaches along the electron-rich cone. In the prospect of future simulations with APMM potentials in drug design or material science, it was thus critical to evaluate if the E_{MTP} contribution, without any extra fitting and/or fictitious center, could reproduce the angular features of halogen bonding. We have thus resorted to a divalent cation, Mg(II), as a probe of the CX bond ($X=\text{F}, \text{Cl}, \text{Br}$) [53] in halobenzenes. A doubly charged species was deliberately chosen to exacerbate the impact of the sigma hole on the angularity of ΔE . The Mg-X distance, d , was first optimized for an approach at theta (C-

X—Mg) of 180° . This was followed by in-plane variations of theta and by out-of-plane of the phi angle describing rotations of Mg(II) on a cone at fixed d and optimized theta (see figures 4). RVS energy-decomposition showed the E_C to be the essential contribution to the angularity of $\Delta E(\text{HF})$. Would its representation going as far as distributed quadrupoles enable E_{MTP} to match E_C ? This is evaluated in figures 5a-b. Figure 5 confirms this to be the case all throughout for all three halogens: for both Cl and Br, there is a pronounced maximum at 180° and two accented minima: in the $105\text{-}120^\circ$ and $240\text{-}255^\circ$ regions for Cl and more accented ones at 105° and 255° for Br. In marked contrast, the curve is for F shallow over the whole $135\text{-}225^\circ$ region. It is also possible to unravel the origin of both the angularities of the Cl and Br curves, and of the shallowness of the F curve. Thus figures 6a-c separate each E_{MTP} curve into its charge-charge (CC), charge-dipole (CD), and charge-quadrupole (CQ) components. The angularities of the Cl and Br curves is clearly dominated by CQ overcoming the opposed preferences of both CC and CD. Possibly just because of its featurelessness, the F curve is revealing. It shows that the flat behavior of E_{MTP} is due to a near-exact compensation between the antagonizing angular features of CQ on the one hand and of CC and CD on the other hand. This is an important *a posteriori* and not taken for granted demonstration that the three components are correctly balanced within E_{MTP} .

For the out-of-plane variations of phi, E_{MTP} again displayed parallel features to E_C . Thus for both Cl and Br, one maximum for found at 180° , and two minimum-energy regions at $60\text{-}120^\circ$ and $240\text{-}300^\circ$. For F, the curve was virtually flat throughout.

We have performed a similar evaluation now with a water probe approaching through either one H atom or through its O atom. For all three halogens, and for theta as well as for phi variations, E_{MTP} could invariably match the angular features of E_C .

6) *Could there be departures from spherical symmetry around some metal cations?* In the polyligated complexes of metal cations, the ligand cations could justifiably be anticipated to bind around a 'crown' surrounding the cation. On account of the spherical symmetry of the cation, this is largely borne out experimentally and computationally in the vast majority of cases, but could there be exceptions? A notable exception is indeed provided by the Pb(II) cation, which in some instances is prone to prefer '*hemi-directed*' arrangements, namely all ligands on one side of the cation, over '*holo-directed*' ones, namely all ligands over the whole

periphery of the cation (Figure 7) [54]. To what an extent could be this be accounted for, if at all, by an APMM approach?

Table I reports the results of SIBFA versus HF comparisons for Pb(II) complexes with 4, 5, and 6 water ligands in the *hemi*- versus *holo*-directed arrangements [55]. The QC/RVS results indicate a small preference in favor of the *hemi*-directed arrangements, decreasing from 6.1 to 4.8 to 1.6 kcal/mol upon passing from 4 to 6 of out 160-200. $\Delta E(\text{SIBFA})$ is able to match this trend, accordingly decreasing from 3.6, to 2.8, to -1.5 kcal/mol. The preferences favoring the *hemi*- arrangements can in SIBFA be traced back to the Pb(II) polarization energy, that is, in its absence, such arrangements would have lesser stabilities than the *holo*- ones. This is consistent with the RVS analyses. It translates the large dipole polarizability of Pb(II), biasing the arrangements towards the *hemi*-arrangements since in the *holo*- ones, the summed electrostatic field polarizing the cation has near-zero values. It is thus fitting to observe that while for the mono-ligated complexes of a cation such as Zn(II) Epol had a limited in-plane directional character, in the polyligated complexes of Pb(II), it is the dominant factor in favor of directionality.

B. Non-additivity.

1) Sign and magnitude of δE_{nadd} . Non-additivity is a critical feature of ΔE . That, is, in multimolecular complexes, its magnitude differs from the sum of its magnitudes in all bimolecular (pair-wise) complexes considered separately. Non-additivity could either increase or decrease the stability of the complexes, resulting into cooperativity or anticooperativity, respectively: these two cases are mostly encountered in multiply hydrogen-bonded complexes and in polycoordinated complexes of metal cations, respectively. The onset of non-additivity, δE_{nadd} , was realized in the earlier stages of development of polarizable potentials. However, to our knowledge until the early nineties there have been surprisingly few, if any at all, attempts to quantify δE_{nadd} on model complexes by QC computations and the separate weights of the $\Delta E(\text{QC})$ contributions, let alone evaluate if PMM were able to reliably match δE_{nadd} . This could be traced back to the fact that with the sole exception of the RVS method, all available energy decomposition procedures are limited to bimolecular complexes. Thanks to this procedure, we could consider several multimolecular complexes and address such points. Such QC/SIBFA comparisons date back from the mid-to late nineties and have borne on: a) mono-, bi-dentate, and through-water complexes of Zn(II) with formate and first- and second-shell waters [56]; polycoordinated complexes of Zn(II) with water [48], and water, hydroxy,

methanethiol and/or methanethiolate ligands [57]; b) polyligated complexes of Zn(II) with the end side-chains of proteins and some Zn-ligating groups of metalloprotein inhibitors [58]; c) several representative water oligomers [49, 59] and d) the complexes of N-methylformamide in an array of linear H-bonded complexes as encountered in models of multilayered β -sheets [60]. The most important conclusions were:

a) With all ligands in the first coordination shell, polycoordinated complexes of divalent metal cations are anticooperative. E_{ct} has a greater anticooperativity than E_{pol} , undergoing a smaller increase in magnitude than E_{pol} upon increasing the coordination number n . A different outcome however occurs in through-water complexes, where for both contributions, a balance between cooperativity and anticooperativity can occur. Both $E_{pol}(\text{SIBFA})$ and $E_{ct}(\text{SIBFA})$ can match the behavior of their RVS counterparts upon increasing n , regarding their magnitudes, extent of non-additivities, and dependence upon the number of ligands in first second shells. As an illustration, we give in Table II a comparison between the QC and SIBFA computations for the complex of Zn(II) with six water molecules. The three considered complexes have either 0, 1, or 2 second-shell water molecules. There is a close correspondence between the SIBFA and QC contributions. As noted originally concerning the best-bound $[\text{Zn}(\text{H}_2\text{O})_6]^{2+}$ complex [48,57], while the number of ligand has increased by 6, E_{pol} and E_{ct} with both RVS and QC have increased in magnitude by factors of only 2.6 and 2 with respect to their corresponding values in the monoligated $[\text{Zn}-\text{H}_2\text{O}]^{2+}$ complex at the optimized Zn-O distance of 2.10 Å found in the hexamer. This, and several other related examples [56, 57, 61] give a clear indication of anticooperativity and of its control by both SIBFA E_{pol} and E_{ct} . This could have been expectable regarding E_{pol} , but was not granted for E_{ct} : it shows that the formulation of E_{ct} embodying dependencies upon the electrostatic potential and field undergone by the electron donor as well as by the electron acceptor can reliably ensure for this critical feature.

b) Multiply H-bonded complexes are generally cooperative. E_{pol} is the dominant, but not unique, contributor to δE_{nadd} . Cooperativity is optimized in cyclic structures if each molecule can act simultaneously as an H-bond donor with one neighbor and as an H-bond acceptor with the other. Anticooperativity was also noted with one cyclic water tetramer [59b], in which one water molecule acts as an H-bond acceptor from both neighbors. Again, both E_{pol} and $E_{ct}(\text{SIBFA})$ could closely match their QC counterparts. In large oligomers ($n=12$ and beyond) having an ice cube-like structure, cooperativity results into a significant compression of the structures, several H-bonded distances shortening by up to 0.2 Å. The dominant magnitude of E_{MTP} becomes strongly opposed by E_{rep} , and thus E_1 attains a much smaller magnitude than

E_{pol} and in some cases even than E_{ct} . The fact that in such complexes E_2 could have a significantly larger weight than E_1 does not appear to have its pendant with *any* other competing PMM potential, yet is fully supported by RVS computations [49, 59a].

c) It is also possible to evaluate, within E_{pol} , the contribution to δE_{nadd} of the iterative calculations of the induced dipoles. The polarizing field is a vector quantity and the polarization energy of a given center is proportional in first approximation to the square of the field it undergoes. Non-additivity thus appears already when the field is computed with the permanent SIBFA multipoles and its magnitude is close to the corresponding magnitude of $E_{\text{pol}}(\text{RVS})$. This is consistent with the fact that in the RVS approach each monomer is considered in turn and relaxed in the presence in the frozen MO's of all the others. At the outcome of the iterative calculation of E_{pol} taking into account the additional contributions of the induced dipoles, E_{pol} has values that are now close to those of $E_{\text{pol}}(\text{QC})$ calculated in a fully variational manner. We have found that in both cooperative and anticooperative complexes at equilibrium, the contribution to δE_{nadd} of the iterative procedure was generally close to 30%, and consistently enforced the preexisting cooperativity or anticooperativity.

-2) On the need for off-centered polarizabilities. The importance of having off-centered polarizabilities, specifically on the tips of saturated lone-pairs, was shown in a study that bore on three model water oligomers [59c]. They were denoted as bifurcated, transverse H-bonded, and longitudinal chains of helical shape (Figure 7). For all three complexes, the SIBFA calculations enabled to reliably reproduce both the magnitude of $E_{\text{pol}}(\text{QC})$ and the values of the total dipole moments. This is due to the fact that in such complexes polarizable centers on the lone-pairs can be closer to an incoming molecule than the bearer atom, and thus sense a more intense field than it. This constitutes an illustrative example of the impact of non-anisotropy on non-additivity. This is a reverse situation to the one encountered in the Pb(II) oligohydrates, for which it was the non-additive behavior of Pb(II) polarization that resulted into non-isotropy.

-3) Impact of quadrupolar polarizabilities. E_{pol} stems predominantly from the dipolar polarizabilities. There are cases, however, in which the polarization energy of some atoms can be increased due to their quadrupolar polarizabilities, whereby quadrupoles can be induced by the gradient of the field. This was observed with the Cu(I) cation [62]. We have compared several Cu(I) di- and oligo- planar ligated complexes in which the ligands are at equal distances from Cu(I) and on opposite sites. In such arrangements the field at the cation

position is null, and so would $E_{\text{pol}}(\text{Cu})$ if it were limited to the sole Cu(I) dipole polarizability. On the other hand the field gradients are non-null, resulting into a significant Cu(I) quadrupolar polarization, the inclusion of which enabled an improved agreement with $\Delta E(\text{QC})$. Only few attempts to include quadrupolar polarizabilities in PMM potentials have been reported so far [63].

-4) Handling intramolecular polarization and the issue of multipole transferability. A large flexible molecule is assembled from its molecular fragments as follows: X and Y denoting two heavy atoms, two successive fragments, F_a and F_b , connect at the level of their X-H and H-Y bonds to create a junctional bond X-Y. The multipoles on the two H atoms and at the centers of the two X-H and H-Y bonds disappear and give rise to multipoles on X, Y, and the mid-point of the X-Y bond, according to proportionality rules related to their distances from these three centers. This preserves the net charge of the assembled molecule, but not that of the individual fragments. This is of no consequence for the calculation of E_{MTP} , since the interactions of the charges along the junction bond connecting F_a and F_b are not computed anyway in SIBFA between the two fragments, although they are indeed with all the other fragments: the 'missing' interactions have no impact upon performing torsions around the junction bond, since they are located along this very bond. A different situation arises for the computation of E_{pol} , because F_a would be polarized by the field of F_b now bearing a non-net charge (0, -1, 1 for neutral, anionic or cationic), and conversely. This would again be immaterial were it not for the presence of other fragments in a larger molecule. The summed field polarizing F_a would be that of a non-net charge before being squared, so that due to non-additivity the residual non-net charge could lead to uncontrolled over- or underestimations of E_{pol} . These would be further amplified by the fact that F_a would be polarized by a centroid at a very close distance from it, namely half the length of the XY bond. Therefore we resorted to an alternative representation. Both HX and HY bonds are shrunk, each H atom being superimposed over its 'bearer' X or Y atom. All polarizing centers thus retain their net initial charge and their shortest distances from the neighboring fragments have lengths never smaller than those of XY bonds. Such a procedure should be more immune to short-distance artifacts. It has been evaluated by several comparisons with QC in a diversity of cases. We have thus compared the conformational energies, δE_{conf} , of ten alanine tetrapeptides put forth by Beachy et al. [64] to evaluate the accuracies of MM force-fields. In our published study [65] the ten conformers differed by their sole torsion angles, i.e. with rigid constitutive fragments, pending completion of the SIBFA stretching and bending harmonic potentials. Inclusion of E_{pol}

enabled the relative SIBFA δE_{conf} values to closely reproduce the corresponding QC values for all ten conformers. Refinements presently underway bear on the representation of the π lone pairs of the prime constituent of the peptide backbone, the N-methylformamide moiety, to further improve the accuracy of the intra-molecular short-range contributions E_{rep} and E_{ct} ; this leads back to the issue of non-isotropy. We have also investigated the conformational dependency of: Na^+ binding to conformers of glycine and the glycine zwitterion [66]; Zn(II) binding to mercaptocarboxamides [67], which constitute the Zn-binding moiety of some Zn-metalloenzyme inhibitors; and Zn(II) binding to tetra-anionic triphosphate, which is the backbone of ATP [68]. The comparisons with the QC results constituted revealing tests of the procedure, requesting the simultaneous and consistent computation of *both* intra- and intermolecular polarization and charge-transfer effects. They enabled to address the issue of multipole transferability [69]. Namely, a limitation of the use of distributed multipoles in intramolecular studies would reside in the variation of their intensities, thus lack of transferability, following conformational changes. The results of our above-mentioned studies on the other hand showed that, exactly as in intermolecular interactions between fragments unconnected by covalent bonds, E_{pol} enables to account for the consequences of conformational changes on *both* δE_{conf} *and* the intermolecular interactions with additional molecules. This occurs provided that: -the permanent multipoles of the constitutive unconnected fragments are the ones used to compute first-order electrostatics; -and the H atoms are carried back on their 'bearer' X and Y atoms of the XY junction bond. Very recent tests have borne on the solvation energies of four inhibitors of the PMI Zn-metalloenzyme, which embody a dianionic phosphate and a monoanionic Zn-binding hydroxamate. Shells with 64 waters were considered and up to 26 complexes in different conformations. Despite the large magnitudes of the interaction energies, the large number of interacting partners, and the diversity of binding modes, close agreements between SIBFA and QC calculations at both HF and correlated levels were demonstrated [Gresh et al., to be submitted].

5) ***Could the first-order exchange repulsion contribute to non-additivity?*** The short-range exchange-repulsion between two molecules is due to reorthogonalization of their MO's upon complex formation. This leads to a destabilization of the total energy of the complex in first-order counteracting the Coulomb contribution. In a multimolecular complex, the energy cost due to simultaneous reorthogonalization can be expected to differ from that due to the summed separate pair-wise reorthogonalizations. The resulting non-additivity of E_{exch} was found to be very small, except for the polyligated complexes of some metal cations. In the

context of SIBFA, it was formulated under the form of a three-center exponential involving the cation and all pairs of ligating heteroatoms, calibrated beforehand on model diligated cations, and then validated by QC comparisons on tetra- and hexaligated complexes [70]. The impact of the non-additivity of $E_{\text{exch}}/E_{\text{rep}}$ is illustrated in the case of one metal cation for which it is the most pronounced, a heavy toxic metal, Hg(II). We have thus considered the tetrahydrated $[\text{Hg}(\text{H}_2\text{O})_4]^{2+}$ complexes in competing square-planar versus tetrahedral arrangements (Figure 7). The results are reported in Table III. The three-body repulsion $\Delta E_{\text{three-body}}$ is 3 kcal/mol larger in the square planar arrangement than in the tetrahedral one. For both arrangements its values computed by SIBFA were close to the QC ones. Its explicit inclusion in SIBFA enabled to account for the preference of Hg(II) in favor of a tetrahedral arrangement. The energy difference between the two arrangements might appear small, but could nevertheless be sufficient to bear on the structural preferences found at the outcome of large-scale MD or MC simulations.

Applications.

1) Conformational study of a polyconjugated drug. Interplay of cooperativity, anisotropy, multipole transferability, and conjugation.

Several drugs which target proteins involved in disease embody conjugated or aromatic groups connected together by conjugated or partly conjugated bonds. This is the case of an inhibitor of neuropilin-1 (NRP1), a protein which when overexpressed is involved in diseases such as cancer or macular degeneracy [71]. A ligand, denoted as Lig-47, was identified in one of our Laboratories after experimental high-throughput screening, and shown to be endowed with a submicromolar activity on several cell lines [72]. Its structure is represented in Figure 9. It is made out of the following chemical groups: benzimidazole, methyl benzene, carboxythiourea (CTU), and benzene-substituted dioxane. It is a highly conjugated drug, and the connections between its four groups all involve unsaturated atoms having sp or sp^2 hybridization. The three-dimensional structure of NRP1 is known from high-resolution X-ray crystallography [73], but not that of its complex with Lig-47. As a prerequisite to APMM MD or MC studies on the NRP1-Lig-47 complex, it is essential to control the ligand conformational flexibility, which is mostly governed by torsions around conjugated bonds. Overestimating it would result into too 'floppy' a ligand and the onset of a manifold of unlikely candidate protein-binding poses. Conversely, underestimating it would give rise to an unrealistically stiff ligand, unlikely to favorably bind its receptor. It was thus imperative to

ensure if the SIBFA δE_{conf} calculations were reliable when compared to the QC ones. The work published in [74], focused essentially on the central CTU unity, and it proceeded along several successive steps:

a) The distributed multipoles and the polarizabilities were derived from the MO's of the constitutive fragments of Lig-47, namely benzimidazole, methyl-benzene, CTU in an extended conformation, and benzene-connected dioxane. The location of the sp^2 lone-pairs of CTU was determined on the basis of ELF [75] analyses using the TopMod package [76], and is shown in Figure 10;

b) For all four constitutive fragments, we calibrated the increments or decrements of the effective van der Waals (vdW) radii of the atoms along their lone-pair directions by probing them with an incoming water probe approaching through one of its H atoms, in order for $E_{\text{rep}}(\text{SIBFA})$ to match $E_{\text{exch}}(\text{RVS})$ over the range of energy-relevant distances;

c) Having set the increment of the vdW radii, CTU was split into four pseudo-fragments. The first and the third one are an sp^2 amine, the second one is thioaldehyde, and the fourth one is aldehyde. In this process fictitious connecting H atoms are created which are given null multipoles, the centroids of each of the two connecting bonds making up a junction are superimposed at the mid-point of the bond and given half the multipoles and polarizabilities of the original bond centroid prior to splitting. CTU thus retains its net initial charge of 0. 15° step-wise variations are performed around the four junction bonds, and the values of one- and two-fold rotational barriers V_0 are calibrated so that $\delta E_{\text{conf}}(\text{SIBFA})$ reproduces $\delta E_{\text{conf}}(\text{QC})$. CTU is then integrated in the entire Lig-47 ligand. The torsional variations are redone to evaluate the transferability of V_0 , for which only limited changes were found necessary. The values of V_0 for the rotations around the junctional bonds connecting CTU to methylbenzene and dioxane, and methylbenzene to benzimidazole were similarly calibrated with respect to QC. In all cases, the curves of $\delta E_{\text{conf}}(\text{SIBFA})$ were found to reproduce very satisfactorily the corresponding QC ones.

Steps a-c are virtually exclusively fitting steps, but which accuracy is to be expected upon passing to a real validation step? This was carried out as follows. We selected all conformations which, for rotations around all junction bonds, corresponded to local minima or to the global one. For each of them, we performed energy-minimization with the 'Merlin' minimizer [77] on all torsional angles

simultaneously. We were thus able to characterize up to 20 distinct conformations. The four most relevant ones are represented in Figure 11. The most stable one, denoted 1b, has an intramolecular H-bond between the NH bond of the first thioamide group of CTU and the carbonyl bond of its formamide group. In figure 12 are plotted the SIBFA and QC δE_{conf} curves. The following analyses will be limited to the HF level. Calculation at the correlated level and with E_{disp} contribution in the SIBFA calculations led to the same conclusions as those to follow. While 1b is confirmed by the QC calculations to be the lowest-energy minimum, its relative stability is clearly underestimated by $\delta E_{\text{conf}}(\text{SIBFA})$ compared to $\delta E_{\text{conf}}(\text{QC})$. The overall R^2 coefficient is 0.88. Could this be improved? CTU had been used as one single building block in an extended conformation enabling to account for the impact of conjugation on the multipoles and polarizabilities. This disables, however, the computation of E_{pol} between the four pseudo-junctions. Firstly, the intramolecular polarization of CTU, which took place during the variational HF procedure, is inherently embodied. Secondly, since the sub-fragments bear non-net charges, and for the reasons mentioned above, attempts to include E_{pol} can be easily anticipated to severely overestimate it. We thus sought for an alternative representation, in which CTU is built from two separate fragments, thioamide and formamide. This enables for their mutual polarization simultaneously with the other Lig-47 fragments, although at the cost of the loss of conjugation between them. The two fragments were again split as before into two pseudo sp^2 amine, one pseudo thioaldehyde and a pseudo aldehyde fragment. The one- and two-fold V_0 torsional barriers were refit as above, and the values of δE_{conf} for the twenty minima were recomputed. The corresponding $\delta E_{\text{conf}}(\text{SIBFA})$ curve is plotted in Figure 13-a along with the QC one, now showing a very close superposition and a R^2 coefficient of 0.96. Figures 13-b and 13-c represent the corresponding evolutions of δE_1 and δE_2 . It is clearly seen that the evolution of $\delta E_{\text{conf}}(\text{SIBFA})$ is governed by E_2 and not by E_1 . While E_{pol} can be shown to be a leading determinant in several cases of molecular recognition, the finding that it plays *the leading role* in shaping the conformational energies of some conjugated molecules has no precedent. Several papers have mentioned [78] that in order to treat polyconjugated compounds, introduction of couplings between successive torsion angles was

necessary. Those studies were done using non-polarizable potentials. Such results might have to be reconsidered since such couplings might have been accounted for by polarization effects which are non-additive and long-range.

2. Binding of halobenzene derivatives to a recognition subsite of the HIV-1 integrase. Joint involvement of anisotropy and non-additivity. The HIV-1 integrase (INT) is a viral enzyme responsible for the integration of the viral DNA genome into the genome of the host cell. It is the target for the development of novel antiviral drugs. Three of these are currently used in therapy, and all three have a halobenzene ring: raltegravir, dolutegravir, and elvitegravir [79]. The high-resolution structure of their complexes with the DNA-bound integrase of Moloney foamy virus has been solved by X-ray crystallography [80]. This INT has very close homologies to the HIV-1 one, enabling inferences from structure-activity relationships for drug design. We have focused first on elvitegravir (EVG), the chlorofluorobenzene ring of which interacts with a guanine-cytosine (GC) base-pair in an INT recognition subsite (Figure 14-a-b). Figure 14-b shows that on the one hand, the electron-deficient prolongation of the C-Cl bond points towards the electron-rich ring of guanine, and that on the other hand, an area of its electron-rich cone can interact favorably with an electron-deficient region around the extracyclic N_4H_2 zone of cytosine. The double-faceted, 'Janus-like' property of the CX bond in halobenzene could be leveraged to enhance its affinity for each of these two regions separately, upon resorting to electron-withdrawing and to electron-donating groups, respectively [81]. A simultaneous enhancement for both sites could even be sought for. Figure 15 gives the structures of several substituted halobenzene candidates. Their interaction energies with the G-C base-pair were optimized by QC calculations at the B97-D level, and relative energy balances were done which took into account their desolvation energies. Several derivatives were found endowed with more favorable energy balances than the parent fluorochlorobenzene ring of EVG, including one, compound H, having both an electron-donating and an electron-withdrawing ring. While the search for improved first-order electrostatics due to anisotropy was indeed justified by the energy decomposition analyses as well by QC-derived contours of Molecular Electrostatic Potential (MEP)

[81], an unanticipated result concerned the role of non-additivity now coming into play on two counts: a) the intermolecular interaction energies in the trimeric complexes could in some cases significantly differ from the sum of the pairwise interactions in the three dimeric complexes. While this has been documented in previous work on multiply H-bonded complexes, it was unprecedented in the case of stacking interactions; b) the energy gains resulting from di- and polysubstitutions could differ from the summed gains resulting from monosubstitutions. To what an extent could APMM account for such QC results [82]? E_{MTP} was shown above to account faithfully for the anisotropy of E_C in halobenzene binding, but is non-additivity still in control for the considered trimeric complexes, which could either involve cooperativity and anticooperativity? The values of the nonadditivities are compared in Table IV for the QC and SIBFA computations. $\delta E_{nadd}(SIBFA)$ reproduces correctly the trends of $\delta E_{nadd}(QC)$, whether cooperative or anticooperative. There is a close agreement between $E_{pol}(RVS)$ and $E_{pol}(SIBFA)$ prior to iterating on the induced dipoles, as also noted from previous publications. $E_{pol}(KM)$ resulting from the Kitaura-Morokuma procedure [83] has greater δE_{nadd} values than found from SIBFA after iterations on the induced dipoles, but this might be caused in part by the non-orthogonalization of the MO's by this procedure. We have considered a total of 18 complexes of compounds selected from Figure 15 with the G-C pair as well as with G and C separately, for which we monitored the evolutions of E_1 , E_2 , and their ΔE sums in Figures 16a and 16b for the SIBFA and QC computations, respectively. The three SIBFA energies closely match the corresponding QC ones. This is also the case for the individual E_{MTP} , E_{rep} , E_{pol} , E_{ct} and E_{disp} contributions [82] and for ΔE_{tot} as compared to $\Delta E(QC/B97-D)$ (Figure 16c). These figures clearly show that both E_1 and E_2 are needed to confer its shape to ΔE . Moreover, we found that for all 18 complexes, whether ternary or binary, the stabilization due to E_2 is larger in magnitude than that due to E_1 . This is reminiscent of the situation with the water oligomers in ice-like arrangements. Here again, the dominant magnitude of E_{MTP} and E_C are counteracted by those of E_{rep} and E_{exch} . The present results indicate that ab initio QC-derived multipoles and polarizabilities can be necessary to control *both* non-isotropy and non-additivity. The latter feature also concerns the gains or losses in binding energies from

polysubstitutions relative to the summed monosubstitutions, the impact of which on the MO's can be reflected by the distributed QC multipoles and polarizabilities whence they are derived.

3) *Structural waters in and around protein recognition sites. Impact of the second-order contributions.*

Discrete water molecules, whether individually or in arrays, are considered to be an integral part of protein or NA structures. We summarize below recent findings aiming to unravel the impact of polarization and charge-transfer on the stabilization energies they confer. These studies bore on superoxide dismutase (SOD), a bimetallic Zn/Cu metalloenzyme, and on the complexes of inhibitors with the FAK tyrosine kinase and with the PMI Zn-metalloenzyme.

a) Superoxide dismutase. SOD is a bimetallic enzyme catalyzing the dismutation of O_2^- into dioxygen and hydrogen peroxide [84]. It is essential for the survival of cells, but even more so for the cancer cells. SOD is thus an emerging target for the design of novel anticancer strategies [85] including photodynamic therapy which can involve Ru(II)-based compounds [86]. Its high-resolution structure has been solved by X-ray crystallography [87] showing the presence of several structural waters in close vicinity to the Zn/Cu binding site. This is an incentive to evaluate whether an APMM approach could single out some privileged water network(s), and the possible extent of its/their overlap with the one found experimentally. As a first step toward such an evaluation [88], we started from the X-ray structure retaining eleven well-defined structural waters, and completed the solvation with up to 296 waters. We then performed short-duration MD runs at temperatures in the 10-300 K range with a simplified SIBFA potential and constrained the waters in a 22 Å sphere centered around Cu(I) using a quadratic potential. We selected six snapshots, denoted *a-f*. For each we then retained the 64 waters closest to Cu(I), and performed energy-minimization (EM) on their positions, on the side-chain conformations of the SOD residues making up, or neighboring, the Zn/Cu binding site, and on the positions of the two cations. Model binding sites were then extracted at the outcome of EM for validation by parallel SIBFA and QC computations. These encompassed selected the main-chains

and/or the side chains of 25 residues, the two metal cations and the 28 closest waters, totaling 301 atoms. Single-point computations were done for validation by parallel QC and SIBFA computations.

Figure 17a gives a representation of the most stable of the six energy-minimized structures, namely *c*. *c* is the structure for which the water networks have the greatest overlap with the one determined by X-ray crystallography used as a starting structure, despite the 'scrambling' it underwent by the initial MD steps. Figure 17b shows a close-up on the water network. There is a dense array of waters connecting two ionic residues, Glu131 and Arg141, which are located beneath the bimetallic site and are at about 10 Å distance from one another. These residues are connected, in fact, by several intermeshed water networks, which are also channeled in other vicinal regions, such as between the side-chains of residues Thr56 and Asn137. These two residues are linked together by a five-water near-linear array, the first and the last of which interact with the dense Glu131-Arg141 connecting water network. Six waters have dipole moments (μ) greater than 2.70 Debye, which is the value found for water oligomers in ice using SIBFA [59a]. High values of the dipole moment were also found for discrete waters in the recognition site of FAK kinase which similarly mediated the interactions between ionic sites. This is mentioned below. Parallel SIBFA and QC computations were performed on complexes *a-f* in the presence and in the absence of the water networks. This enabled to compute the stabilization brought by the water networks. Figure 18a displays the evolutions of $\Delta E(\text{SIBFA})$ and $\Delta E(\text{HF})$ in the six complexes. The evolution of $\Delta E(\text{HF})$ is very closely matched by that of $\Delta E(\text{SIBFA})$, the relative errors being <2%. As was the case for substituted halobenzene binding to the G-C base pair of HIV-1 integrase, both E_1 and E_2 terms are necessary to confer its proper shape to ΔE . The superimposition of $\Delta E(\text{QC/B97D})$ and $\Delta E_{\text{tot}}(\text{SIBFA})$ curves is even better at the correlated level (Figure 18b). One means to validate the high values of the dipole moments found for water is to compare the total values of μ in the six 28-water clusters extracted from complexes *a-f* (retaining a net charge of 0 ensures that the dipole moment is translation-independent). Figure 19 compares the evolutions of μ as derived from both QC and SIBFA in the six clusters, with a close and clear

correspondence. The R^2 factor is of 0.99. It is also seen that the most stable complex, *c*, is the one for which μ has the highest value, attesting to the importance of polarization and non-additivity in its preferential stabilization.

We stress again that the close agreements found for SIBFA with $\Delta E(QC)$ at both HF and correlated levels could only be possible thanks to the separable nature of the potential, a proper balance of first- and second-order contributions, and control of non-additivity in large complexes. They are encouraging in the perspective of long-time MD simulations, enabled by very important recent advances in the development of a highly efficient and scalable code by one of our Laboratories [89]. We thus plan to monitor the lifetimes of the individual waters in the networks, the possible existence of other, competing networks, the possibility of their mutual interconversions, and the channeling of solutes toward the bimetallic site.

b) Focal Adhesion Kinase (FAK). Kinases presently account for about 40% of the targets for drug design [90]. They are a class of enzymes which draft a phosphate group from ATP to hydroxylated amino-acids, namely tyrosine, serine and threonine. This results into cellular activation but also if overexpressed into pathologies such as cancer, arthrosis and neurodegenerative diseases [91]. FAK is a Tyr kinase which subsequent to autophosphorylation, can trigger a cascade of protein-protein interactions resulting into signal transmission to the cellular nucleus to trigger cell division and motility. Its three-dimensional structure has been resolved by X-ray diffraction showing the ATP-binding site in a hinge between the N- and C-terminal lobes (Figure 20) [92]. Five inhibitors in the pyrrolopyrimidine were designed, synthesized and tested by the Novartis company [93]. They all have in common a benzene substituting the five-membered ring nitrogen. The benzene is substituted by a carboxylate group at the *ortho* or *meta* position. In the latter, there are 0, 1, or 2 methylene groups interposed. They are represented in Figure 21, along with their IC_{50} values in μM and using the notations of the original paper. Compound *16i* with an *ortho* carboxylate substituent is the least active (16 μM). Compounds *17g*, *17h*, *17i* all have a *meta* carboxylate substituent and have the same

submicromolar affinity (0.04 μM), ie a two-order-of-magnitude enhancement in affinity. A further gain results from the replacement of benzene of *17i* by pyridine, with compound *32* now nanomolar ($\text{IC}_{50}=0.004 \mu\text{M}$). Thus, apparently modest structural changes can result into very large (thousand-fold) changes in the binding affinities. Could APMM procedures shed light on the factors governing such large changes [94]? Energy-minimizations were performed in which the solvation free energy was computed by a Continuum reaction field procedure, which was designed by Langlet, Claverie and their coworkers [95]. We denote this contribution as $\Delta G_{\text{solv}}(\text{LC})$. The solvent is represented by a 'bulk' which responds to the electrostatic potential generated by the solute on its van der Waals by creating fictitious charges, which interact with the solute potential to give rise to the electrostatic contribution of $\Delta G_{\text{solv}}(\text{LC})$. The energy balances take into account: a) on the one hand: the intermolecular ligand-protein interaction energy and the solvation energy of the complex; and b) on the other hand, the conformational energy costs of the ligand and of the protein upon passing from their uncomplexed, solvated states to the complex, along with their corresponding desolvation energies. An overlay of the five complexes in the recognition site after energy-minimization is given in Figure 22, showing an extensive overlap except at the position of the ligand carboxylates. The energy balances are given in Table V under the form of differences between a) and b) for each contribution. They show no correlation at all with the experimental results. Thus, eg, there is 7 kcal/mol energy difference disfavoring compound *32*, which is nanomolar, with respect to *17h*. Yet *17h* has a ten-fold lesser experimental affinity than *32*; and there is an 11 kcal/mol energy difference between *17g* and *17h* which in fact have similar experimental affinities. Separate QC tests on the FAK recognition site having confirmed the accuracy of the SIBFA procedure, we were led to evaluate the extent to which a limited number of 'discrete' waters could impact the relative energy balances. For that purpose, five, six, or seven waters were located in the complexes between each ligand and a reduced model of FAK limited to the recognition site shown in Figure 22. They were initially located thanks to a procedure [96] which minimizes with a simplified energy function a limited number of discrete waters around the accessible hydrophilic sites of the solute. These positions were

reoptimized by a Generalized Simulated Annealing [97] procedure with the SIBFA potential, then minimized with Merlin. The final resulting positions were then ported to the entire FAK and EM redone again in the presence of $\Delta G_{\text{solv}}(\text{LC})$. Figure 23 gives a simplified representation limited to the complex of the end carboxylate of 32, the ionic sites of FAK, and five discrete waters (denoted as complexes 'c_w' in Ref. 94). These waters can clearly snugly fit in the structure. They can either mediate the interactions between the ligand and PMI as occurs with residues Glu471, Arg550 and Asp564, or complement them, as occurs with residue Lys454. Several waters have much stronger dipole moments than ice, so that the polarization energy contribution could be expected to be a key contributor to ΔE . This led us to perform a parallel SIBFA/QC(RVS) analysis of the intermolecular interactions on complexes c and c_w, without and with the discrete waters. The analyses done for the two extreme compounds, nanomolar 32, and micromolar 16i, are reported in Table VI. In the absence of the waters, E₁ favors by 17 kcal/mol 16i over 32, while E₂ favors by 3-4 kcal/mol 32 over 16i. A remarkable reversal in the magnitudes of the preferences takes place in the presence of the discrete waters. E₁ now favors by only 4-5 kcal/mol 16i over 32, but E₂ favors 32 over 16i by a very significantly augmented preference, namely 17 kcal/mol. The resulting preference of 13-14 kcal/mol in terms of $\Delta E(\text{SIBFA})$ and $\Delta E(\text{RVS})$ is thus the one imposed by E₂. The persistent agreements between all SIBFA and RVS individual contributions is noteworthy for all four complexes. The final energy balances in the presence of the five structural waters are given in Table VII. All five ligands are now ranked at least qualitatively along the correct sequence ranking first the nanomolar compound 32, then the three submicromolar compounds 17g, 17h, 17i, and then the micromolar compound 16i. The same conclusions hold with 6 and 7 discrete waters. The critical role of E_{pol} in such balances is noteworthy. The need for E_{pol} for a correct ranking of affinities had been previously shown in a study with the AMOEBA potential that bore on the complexes of trypsin with benzamidine derivatives [98], although its role was possibly not as extreme as in the present study. As an extension of the present work, we plan to resort to a massively parallel version of the TINKER software on which the SIBFA potential is ported to perform long-duration MD. These should enable us to monitor the life-times of

the discrete waters and their rates of exchange with the solvent, and possibly the path for interconversion between 'DFG-in' and 'DFG-out' conformations [99].

c). *Phosphomannose isomerase (PMI)*. PMI is a Zn-metalloenzyme which catalyzes the reversible isomerization of fructose-phosphate into mannose-phosphate [100]. It is responsible for several infectious and parasitic diseases but there is no clinically-useful inhibitor against it [101]. A hydroxamate inhibitor, denoted 5PAH was designed, synthesized and tested in the Laboratory of Bioorganic and Bioinorganic Chemistry at Orsay, France, and shown to display a submicromolar inhibitory potency. By contrast, an analogue with formate replacing hydroxamate was devoid of potency [102]. Based on the X-ray crystal structure of Zn-bound PMI [103, Figure 25], we were able to account for these experimental results and derived a structural model locating the hydroxamate in the Zn-binding pocket and the phosphate at the entrance of the cavity where it binds simultaneously to two cationic residues, Arg304 and Lys310 [104]. In a next step, four ligands in the sugar family were considered (Figure 26) [105]. The first three ones (1-3) have a dianionic phosphate. The first (1) is β -D-mannopyranose 6-phosphate (β -6-MP1). The fourth (4) is an analog of β -6-MP1 but has a malonate with two monoanionic carboxylates replacing the phosphate. Only compound 1 in the phosphate series displayed a measurable PMI binding affinity. The malonate derivative 4 displayed a ten-fold larger binding affinity than it. This could constitute a step toward the design of therapeutically relevant drugs, because malonate is more resistant to enzymatic hydrolysis than phosphate, and is also more easily transported. The SIBFA calculations have enabled to account for the greater affinity for PMI of 1 than 2 and 3. However the energy balances with the sole $\Delta G_{\text{solv}}(\text{LC})$ terms failed to account for the greater affinity of the malonate derivative. This led us, as in the case of FAK, to solvate their complexes with discrete waters. Nine waters were optimized in the PMI-1 and PMI-4 complexes. The structure of the latter is shown in Figure 27. Three networks are found. The first network bridges one O of the most accessible carboxylate of the ligand with Trp18 and Glu48 residues. These interactions are extended by ionic interactions with residues Lys100 and Glu294. The second network bridges the other anionic O with Asp17. The third network bridges the sole

accessible anionic O of the second carboxylate with Arg304 and Asp300. Residues Asp17, Glu48, and Asp300 are at about 18 Å distance from one another. We thus observe an extension of the recognition site to PMI residues that do not interact directly with the ligand, and such an extension is mediated by the polarizable water molecules.

In the complex of I, the phosphate fits more snugly than malonate between Arg304 and Lys310. This on the one hand gives rise to stronger electrostatic interactions with these two residues, but at the price of a lesser accessibility to the structural waters. The differential stability due to the nine waters can be illustrated by comparing the interaction energies of the two ligands in the recognition site. Each site has been extracted from the energy-minimized ligand-PMI complex, and single-point computations were done with and without the nine structural waters. The SIBFA interaction energies are reported in Table VIII and compared to the QC ones. For each contribution and for each ligand, we also report the values of $\delta(a-b)$, namely the gain due to the nine waters. The gain in E_1 is by only -1.6 kcal/mol more favorable for the malonate than for the phosphate ligand. Such relative gains increase very significantly with the second-order contributions, E_{pol} and E_{ctr} , passing to -7.7 and -5.2 kcal/mol, respectively. Thus the networks totaling nine waters would stabilize by -14.7 kcal/mole the malonate ligand over the phosphate one. This value is very close to the corresponding QC(HF) value of -15.7 kcal/mol. Inclusion of dispersion/correlation does not alter the outcome. The comparative energy balances done on the complete ligand-PMI gave rise to the same conclusion: there is a distinct preference in favor of the malonate over the phosphate derivative, but it is only enabled by the networks of structural waters. However, as noted in [105], more exhaustive sampling of the energy surface, along with long-time MD and accounting for entropy effects, are needed for a more quantitative evaluation. This will be further discussed in the last section of this review.

Conclusions and perspectives.

There are numerous fields of application of computational chemistry where next-generation QC-derived anisotropic polarizable molecular mechanics/dynamics could very significantly extend the realm of ab initio quantum chemistry. These encompass, eg, drug design, material science, and supramolecular chemistry. APMM should be able to handle systems with sizes larger by at least four orders of magnitude than QC, and/or enable simulation times also larger by similar orders. But a prerequisite to very large scale applications is an objective evaluation of its expectable accuracy. In this respect, a distinctive asset of the SIBFA procedure, which appears to this day to be shared by

very few other potentials [14], is the separability of ΔE into five distinct contributions, each of which is formulated and calibrated on the basis of its ab initio QC counterpart, and subsequently extensively tested against it.

We have reviewed in this paper the inherent non-isotropy and non-additivity features of several of these contributions, and their impact on overall structure and energetics. The SIBFA procedure has lent itself to numerous confrontations against QC, more so than any other competing method. It could be adequate to conclude to shortly develop on three points: its refinements and enrichments, its integration into highly optimized softwares, and the realm of its applications.

-a) Refinements.

-Regarding electrostatics. The distributed multipoles and polarizabilities used to construct the SIBFA library of fragments were derived from QC fragment calculations using the CEP 4-31G(2d) basis set by Stevens et al. [106]. Accordingly, most validation studies resorted to QC computations using this basis as well. Upon comparing the evolutions of intermolecular interaction energies for a series of different complexes, we found invariably the values of $\Delta E(\text{HF})$ with this base to very closely parallel those with larger basis sets [107], the most extended one being aug-cc-pVTZ(-f) [Gresh et al., to be submitted]. This attests to the high reliability of this basis set, and justifies its use to construct the SIBFA library of fragments. There are several cases, however, where it could be preferable to resort to very extended basis for calibration and validation purposes. Accordingly, we are assembling a new library of fragments with multipoles and polarizabilities now derived from uncorrelated as well as correlated aug-cc-pVTZ(-f) calculations. The parametrization phase can be automatized thanks to the I-NoLLS algorithm [108]. It was recently reported in the context of SIBFA [109]. Once the 'general' parameters are set, the calibration of individual atom types or the introduction of new atoms, such as metal cations, becomes straightforward. This was done recently in the $\text{Li}^+ \text{--} \text{Cs}^+$ alkali cation series [45].

-Regarding short-range. E_{rep} , E_{ct} , and $E_{\text{disp-exch}}$ have dependencies upon the location of the lone-pair tips. Such locations can be derived from QC analyses such as Boys' localization procedure [110] or ELF [75], as analyzed for a series of ligands by Chaudret et al. [111], whence an additional filiation of SIBFA to QC.

-b) Enrichments. Multi-scale approaches such as QM/MM, pioneered in 1976 [6a] constitute nowadays an emerging field of computational chemistry. Steps toward merging SIBFA and the

Gaussian Electrostatic Model (GEM) [112] have been completed [113], and a complete integration of the two approaches is underway. Owing to their polarizable nature, APMM approaches are well suited to a merging with QM approaches. This was completed recently concerning AMOEBA [Piquemal et al., submitted] and could be pursued with SIBFA.

-c) Integration into massively parallel codes. There could be very important perspectives for the use of the SIBFA potential on a much larger scale than before. It is presently being integrated in the newly developed Tinker-HP software. It will therefore benefit from novel algorithmic developments to speed up polarizable molecular dynamics. For example, the bottleneck of the polarization energy and associated derivative evaluation on parallel computers has been overcome by the use of new iterative techniques such as the Jacobi/DIIS approach offering good scaling on hundreds and even thousands processors with gains in time going up to three orders of magnitude upon using advanced MD predictor-corrector algorithms [89]. SIBFA should also benefit from the high performance Smooth Particle Mesh periodic boundary condition implementation for electrostatics, including the short-range penetration correction [114] and for the polarization energy that uses newly introduced solvers and benefits from a $N\log(N)$ scalability [115]. Overall, all derivatives and torques have been coded and production simulation runs could be anticipated to start this year. Moreover, another asset will be the availability of the newly developed domain decomposition Cosmo (dd-Cosmo) continuum solvation model that is now available in direct connection with polarizable molecular dynamics [116]. To conclude on the technical part, new parametrization strategies have been defined with automatic parametrization using the INOLLS software [108]. Such an approach should greatly reduce the time effort required for the definition of new parameter sets [109].

d) Prospective applications.

-Ligand-macromolecule complexes. One of the most attractive fields of APMM applications is ligand-protein complexes. There have been published applications regarding kinases [94] and metalloproteins [88, 105, 117-119]. It could be rewarding to adapt Free Energy Perturbation (FEP) methods [120] or non-equilibrium MD [121] to such targets, and particularly metalloproteins, on account of the demonstrated reliable handling of metal cation-ligand interactions. Along these lines, we note that an AMOEBA application was recently coauthored by one of us, which bore on the binding to MMP-13 of four dicarboxamide inhibitors [120]. This was the first ever reported FEP study on a metalloprotein using polarizable potentials. Although the ligand structural changes bore on sites

distinct from the Zn-binding site, it is expectable that changes directly affecting Zn(II)-binding are amenable to prospective SIBFA FEP calculations.

-Supramolecular chemistry and material science. As reviewed above, SIBFA has been adapted to a diversity of metal cations. These encompass the following: alkali Li(I)-Cs(I) [45], alkaline-earth Mg(II) and Ca(II) [47b], transition metals Cu(I) [62], Cu(II) [44], Zn(II) and Cd(II) [47b, 48, 61], heavy metals Pb(II) [55] and Hg(II) [70], and lanthanides and actinides [122]. On the one hand, this should enable to investigate their binding, stationary or transitory, to a diversity of proteins and NA's. On the other hand, this should enable to address the issue of preferential entrapment of one cation over that of others by a supramolecular host, and possibly the design of cation-selective hosts for extraction or detoxification. The computation of free energies of binding could be based on FEP, non-equilibrium MD, or possibly by computing the contribution of vibrational entropy [123]. Finally, there is a little charted domain of application of APMM approaches, which relates to surfaces and nanostructures. Accessing the values of their distributed multipoles and polarizabilities, along with the handling of Periodic Boundary Conditions (PBC) in SIBFA, and following validations against QC in model systems, could pave the way for numerous studies on adsorption events.

-Modeling of nucleic acids. The application of APMM to nucleic acids constitutes another virtually uncharted ground [see, eg, refs. 124]. Yet NA's are an ideal domain of application for such approaches, considering the polyanionic nature of the sugar-phosphate backbone and the strongly polar and polarizable nature of the bases. Several issues can be mentioned: the structure, organization, and dynamics of the water networks in the groove, the dynamics of binding of metal cations to the backbone, the groove, and/or the water networks; the amplitude of stacking energies of successive base-pairs, from which the sequence-dependent conformation of NA's depend; and the conformational properties of the phosphodiester backbone needing to handle properly polarization and anomeric effects.

Acknowledgments.

We wish to thank the Grand Equipement National de Calcul Intensif (GENCI): Institut du Developpement et des Ressources en Informatique Scientifique (IDRIS), Centre Informatique de l'Enseignement Supérieur (CINES), France, project No. x2009-075009), and the Centre de Ressources Informatiques de Haute Normandie (CRIHAN, Rouen, France), project 1998053. This work was supported in part by the French state funds managed by CALSIMLAB and the

ANR within the Investissements d'Avenir program under reference ANR-11-IDEX-0004-02.
F.L.

References.

- 1.a) Car, R.; Parrinello, M. *Phys. Rev.* **1985**, *55*, 2471; b) Kuhne, T. D.; Krack, M.; Mohamed, F. R.; Parrinello, M. *Phys. Rev. Letts.* **2007**, *98*, 066401.
2. a) Schlegel, H. B.; Iyengar, S.; Li, X., Millam, J. M. ; Voth, G. A. ; Scuseria, G. E.; Frisch, M. *J. Chem. Phys.* **2002**, *117*, 8694; b) Tongraar, A.; Liedl, K. R.; Rode, B. M. *J. Phys. Chem. A.* **1998**, *102*, 10340.
3. a) Titov, A. V. ; Ufimtsev, I. S.; Luehr, N.; Martinez, T. J. *J. Chem. Theory Comput.* **2013**, *9*, 213; b) Ufimtsev, I. S. ; Luehr, N. ; Martinez, T. J. *J. Phys. Chem. Letts.* **2011**, *2*, 1789.
4. Schmidt, M. W., Baldridge, K. K.; Boatz, J. A., Elbert, S. T., Gordon, M. S., Jensen, J. H., Koseki, S., Matsunaga, N., Nguyen, K. A., Su, S., Windus, T. L., Dupuis, M., Montgomery, J. A. *J. Comput. Chem.* **1993**, *14*, 1347.
5. a) York, D, M.; Lee, T.-S.; Yang, W. *Phys. Rev.* **1998**, *80*, 5011; b) Scuseria, G. *J. Phys. Chem. A.*, **1999**, *103*, 4782; c) Nam, K.; Gao, J.; York, D. M. *J. Chem. Theory Comput.* **2005**, *1*, 2; d) Yang, W.; Lee, T.-S. *J. Chem. Phys.* **1996**, *103*, 5674 ; e) Monard, G. ; Berna- Uruchurtu, M. I. ; van der Waart, A. ; Merz, K. M.; Ruiz-Lopez, M. *J. Phys. Chem. A.* **1998**, *109*, 3425; e) VandeVondele, J.; Borstnik, U.; Hutter, J. *J. Chem. Theory Comput.* **2012**, *8*, 3565.
6. a) Warshel, A.; Levitt, M. *J. Mol. Biol.* **1976**, *103*, 227; b) Maseras, F.; Morokuma, K. *J. Comput. Chem.* **1995**, *16*, 1170; c) Senn, H. M. ; Thiel, W. *Angewandte Chem.* **2009**, *48*, 1198; d) Rod, T. H.; Ryde, U. *Phys. Rev. Lett.*, **2005**, *94*, 138; e) Monari, A.; Rivail, J.-L.; Assfeld, X. *Acc. Chem. Res.* **2013**, *46*, 596; f) Ferre, N.; Assfeld, X.; Rivail, J.-L. *J. Comput. Chem.* **2002**, *23*, 610; g) Very, T.; Despax, S.; Hebraud, P.; Monari, A.; Assfeld, X. *Phys. Chem. Chem. Phys.* **2012**, *14*, 12496; h) Antonczak, S.; Monard, G.; Ruiz-Lopez, M. Rivail,

J.-L. *J. Am. Chem. Soc.* **1998**, *120*, 8834; i) Ryde, U.; Olsen, L.; Nilsson, K.; *J. Comput. Chem.* **2002**, *23*, 1058.

7. Gresh, N., de Courcy, B., Piquemal, J.P., Foret, J., Courtiol-Legourd, S., Salmon, L. *J. Phys. Chem. B*, **2011**, *115*, 8304.

8. a) Gresh, N. *Curr. Pharm. Des.* **2006**, *12*, 2121; b) Dehez, F.; Angyan, J.; G.; Soteras Gutierrez, I. S.; Luque, F. J.; Schulten, K.; Chipot, C. *J. Chem. Theory Comput.* **2007**, *3*, 1914; c) Gresh, N.; Cisneros, A. G.; Darden, T. A.; Piquemal J.-P. *J. Chem. Theory Comput.* **2007**, *3*, 1960; d) Warshel, A.; Kato, M.; Pislakov, A. V. *J. Chem. Theory Comput.* **2007**, *3*, 2034; e) Cieplak, P.; F.-Y. Dupradeau, Duan, Y.; Wang, J. *J. Phys. Condens. Matter* **2009**, *21*, 33102; f) J. W. Ponder, C. Wu, P. Ren, V. S. Pande, J. D. Chodera, D. L. Mobley, M. J. Schnieders, I. Haque, D. S. Lambrecht, R. A. DiStasio, Jr., M. Head-Gordon, G. N. I. Clark, M. E. Johnson, T. Head-Gordon, *J. Phys. Chem. B*, **2010**, *114*, 2549.

9. a) Rick, S. W.; Stuart, S. J.; Berne, B. J. *J. Chem. Phys.* **1994**, *101*, 6141; b) Stern, H. A.; Rittner, F.; Berne, B. J.; Friesner, R. A. *J. Chem. Phys.* **2001**, *115*, 2237; c) Chelli, R.; Procacci, P. *J. Chem. Phys.* **2002**, *117*, 9175.

10. a) Lamoureux, G.; MacKerell, A. D., Jr.; Roux, B. *J. Chem. Phys.* **2003**, *119*, 5185; b) Anisimov, V.; Vorobyov, I. V.; Roux, B.; MacKerell, Jr., A. D. *J. Chem. Theory Comput.* **2007**, *3*, 1927.

11. a) Pullman, B.; Claverie, P.; Caillet, J. *Proc. Natl. Acad. Sci. U.S.A.* **1967**, *57*, 1663. b) Rein, R.; Claverie, P.; Pollack, M. *Int. J. Quantum Chem.* **1968**, *2*, 1129. c) Claverie, P.; Rein, R. *Int. J. Quantum Chem.* **1969**, *3*, 537.

12 a) Gresh, N.; Claverie, P.; Pullman, A. *Theor. Chim Acta* **1984**, *66*, 1; b) Gresh, N.; Pullman, A.; Claverie, P. *Theor. Chim. Acta* **1985**, *67*, 11.

13. a) Price, S. L.; Stone, A, J. *Mol. Phys.* **1984**, *51*, 569 ; b) Price, S. L.; Stone, A, J. *J. Chem. Soc., Faraday Soc.* **1992**, *88*, 1755.

14. a) Day, P.; Jensen, J. H.; Gordon, M. S.; Webb, S. P.; Stevens, W. J.; Krauss, M.; Garmer, D. R.; Basch, H.; Cohen, D. J. *Chem. Phys.* **1996**, *105*, 1968. b) Slipchenko, L. V. Gordon, M. S. *J. Comput. Chem.* **2007**, *28*, 276; c) Gordon, M. S.; Fedorov, D. G.; Pruitt, S. R.; Slipchenko, L.

V. Chem. Rev. **2012**, *112*, 632; d) Gordon, M. S.; Smith, Q. A.; Xu, P.; Slipchenko, L. V. *Annu. Rev. Phys. Chem.* **2013**, *64*, 553.

15. Millot, C. J.; Soetens, J. C.; Martins, Costa, N. T. C.; Hodges, M. P.; Stone, A. J. *J. Phys. Chem. A* **1998**, *102*, 754.

16. a) Karlstrom, G.; Linse, P.; Wallqvist, A.; Jonsson, B. *J. Am. Chem. Soc.* **1983**, *105*, 3777; b) Hermida-Ramon, J. M.; Brdarski, S.; Karlstrom, G.; Berg U. *J. Comput. Chem.* **2003**, *24*, 161.

17. a) Ren, P. Ponder, J. W. *J. Phys. Chem. B* **2003**, *107*, 5933; b) Shi, Y.; Xia, Z.; Zhang, J.; Best, R.; Wu, C.; Ponder, J. W.; Ren, P. *J. Chem. Theory Comput.*, 2013, **9**, 4046.

18. (a) Dreyfus, M. Ph.D. Thesis, University of Paris, 1970. (b) Claverie, P. Ph.D. Thesis, Paris, 1973, CNRS library number A.O. 8214. (c) Claverie, P. In '*Localization and Delocalization in Quantum Chemistry*'; Chalvet, O., Daudel, R., Diner, S., Malrieu, J. P., Eds.; Reidel: Dordrecht, Vol. II, p 127.

19. a) Pullman, A.; Zarkzewska, C.; Perahia, D. *Int. J. Quantum. Chem.* **1979**, *16*, 395; b) Pullman, A.; Perahia, D. *Theoret. Chim. Acta*, **1979**, *50*, 351; c) Perahia, D.; Pullman, A.; Pullman, B. *Theoret. Chim. Acta* **1979**, *51*, 349; d) Pullman, B.; Perahia, D.; Cauchy, D. *Nucleic Acids Res.* **1979**, *10*, 3821.

20. a) Lavery, R.; Pullman, A.; Pullman, B., de Oliveria, M. *Nucleic Acids. Res.* **1980**, *8*, 5095; b) Lavery R, Pullman B, Corbin S. *Nucleic Acids Res.* **1981**, *9*, 6539; c) Lavery R, Pullman B, Zakrzewska K.; *Biophys. Chem.* **1982**, *15*, 343.

21. Lavery, R.; Pullman, A.; Wen, Y. K. *Int. J. Quantum. Chem.* **1982**, *24*, 353.

22. Zarkzewska, C.; Pullman, A. *Int. J. Quantum. Chem. Quantum Biol. Symp.* **1982**, *9*, 411.

23. a) Etchebest, C.; Lavery, R.; Pullman, A. *Studia Biophys.* **1982**, *90*, 7; b) Gresh, N.; Pullman, A. *Int. J. Quantum Chem. Quantum Biol. Symp.* **1983**, *10*, 215.
24. Gresh, N.; Claverie, P.; Pullman, A. *Int. J. Quantum Chem. Symp* **1979**, *13*, 243.
25. a) Gresh, N. *Biochim. Biophys. Acta* **1980**, *597*, 345; b) Gresh, N.; Pullman, B. *Biochim. Biophys. Acta* **1980**, *625*, 356; c) Gresh, N.; Etchebest, C.; de la Luz Rojas, O.; Pullman, A. *Int. J. Quantum Chem. Quantum Biol. Symp.* **1981**, *8*, 109; d) Gresh, N.; Pullman, A. *Int. J. Quantum Chem.* **1982**, *22*, 709; .e) Gresh, N.; Pullman, B. *Mol. Pharmacol.* **1984**, *25*, 452; f) Gresh, N. *Biopolymers* **1985**, *24*, 1527.
26. Vigne-Maeder, F.; Claverie, P. *J. Chem Phys.* **1988**, *88*, 4934.
27. a) Rein, R.; Rabinowitz, J. R.; Swisler, T. J. *J. Theor. Biol.* **1972**, *34*, 215; b) Rein, R. *Adv. Quantum Chem.* **1973**, *7*, 335.
28. a) Stone, A. J. *Chem. Phys. Lett.* **1981**, *83*, 233. b) Stone A. J.; Alderton, M. *Mol. Phys.* **1985**, *56*, 1047.
29. a) Sokalski, W. A.; Poirier, R. A. *Chem. Phys. Lett.* **1983**, *98*, 86; b) Sokalski, W. A.; Sawaryn, A. *J. Chem. Phys.* **1987**, *87*, 526.
30. a) Karlstrom, G.; Linse, P.; Wallqvist, A.; Jonsson, B. *J. Am. Chem. Soc.* **1983**, *105*, 3777. b) Andersson, M.; Karlstrom, G. *J. Phys. Chem.* **1985**, *89*, 4957.
31. a) Angyan, J. G.; Chipot, C.; Dehez, F.; Hattig, C.; Jansen, G.; Millot, C. *J. Comput. Chem.* **2003**, *24*, 997; b) Chipot, C.; Angyan, J. H. *New J. Chem.* **2005**, *29*, 2005.
32. a) Freitag, M.; Gordon, M. S.; Jensen, J. H.; Stevens, W. J. *J. Chem. Phys.* **2000**, *112*, 7300; b) Gordon, M. S.; Freitag, M. A.; Bandyopadhyay, A.; Jensen, J. H.; Kairys, V.; Stevens, W. J. *J. Phys. Chem. A* **2001**, *105*, 293.
33. Piquemal, J.-P.; Gresh, N.; Giessner-Prettre, C. *J. Phys. Chem. A* **2003**, *107*, 10353.

34. a) Slipchenko, L. V.; Gordon, M. S. *J. Comput. Chem.* **2006**, *28*, 276; b) Wang, B.; Truhlar, D.G. *J. Chem. Theory Comput.* **2010**, *6*, 3330; c) Stone, A. J. *J. Phys. Chem. A* **2011**, *115*, 7017.
35. Garmer, D. R.; Stevens, W. J. *J. Phys. Chem.* **1989**, *93*, 8263.
36. a) Gresh, N.; Leboeuf, M.; Salahub, D. R. **1994**, in *Modeling the Hydrogen Bond, American Chemical Society Symposia, No. 569*, 82, D. A. Smith, Ed.; b) Jensen, J. H.; Day, P. N.; Gordon, M. S.; Basch, H.; Cohen, D.; Garmer, D. R.; Krauss, M.; Stevens, W. J. *Ibid*, p. 139.
37. Murrell, J. N.; Teixeira-Dias, J. J. C. *Mol. Phys.* **1970**, *19*, 521.
38. Murrell, J. N.; Randic, M.; Williams, D. R. *Proc. R. Soc. London, Ser. A* **1966**, *284*, 566.
39. a) Gresh, N.; Claverie, P.; Pullman, A. *Int. J. Quantum Chem.*, **1982**, *22*, 199 ; b) Gresh, N.; Claverie, P.; Pullman, A. *Int. J. Quantum Chem.* **1986**, *29*, 101.
40. Creuzet, S.; Langlet, J.; Gresh, N. *J. Chim.-Phys. Phys. Chim. Biol.* **1991**, *88*, 2399.
41. Stevens, W. J.; Fink, W. *Chem. Phys. Letts.* **1987**, *139*, 15.
42. Bagus, P. S.; Hermann, K.; Bauschlicher, C. J. *J. Chem. Phys.* **1984**, *80*, 4378.
43. Jeziorski, B.; Moszynski, R.; Szalewicz, K. *Chem. Rev.* **1994**, *94*, 1887.
44. Piquemal, J.-P.; Hubbard, B. W.; Fey, N.; Deeth, R.; Gresh, N.; Giessner-Prettre, C. *J. Comput. Chem.* **2003**, *24*, 1963.
45. Dudev, T.; Devereux, M.; Meuwly, M.; Lim, C.; Piquemal, J.-P. ; Gresh, N. *J. Comput. Chem.* **2015**, *36*, DOI. 10.1002/jcc.23801.
46. Buckingham, A. D.; Fowler, P. W. *J. Chem. Phys.* **1983**, *79*, 6426.

47. Garmer, D. R. ; Gresh, N. *J. Am. Chem. Soc.* **1994**, *116*, 3556 ; b) Gresh, N.; Garmer, D. *R. J. Comput. Chem.* **1996**, *17*, 1481.
48. Gresh, N. *J. Comput. Chem.* **1995**, *16*, 856.
49. Piquemal, J.-P.; Chevreau, H.; Gresh, N. *J. Chem. Theory Comput.* **2007**, *3*, 824.
50. a) Lu, Y.; Shi, T.; Wang, Y.; Yang, H.; Yan, X.; Luo, X.; Jiang, H.; Zhu, W. *J. Med. Chem.* **2009**, *52*, 2854; b) Hernandez, M. Z.; Cavalcanti, S. M.; Moreira, D. R.; de Azevedo, W. F., Jr.; Leite, A. C. *Curr. Drug Targets.* **2010**, *11*, 303; c) Matter, H.; Nazaré, M.; Güssregen, S.; Will, D. W.; Schreuder, H.; Bauer, A.; Urmann, M.; Ritter, K.; Wagner, M.; Wehner, V. *Angew. Chem., Int. Ed.* **2009**, *48*, 2911.
51. a) Clark, T.; Hennemann, M.; Murray, J. S.; Politzer, P. *J. Mol. Mod.* **2007**, *13*, 291; b) Murray, J. S.; Lane, P. Politzer, P. *J. Mol. Mod.* **2009**, *15*, 723; c) Politzer, P.; Murray, J. S.; Clark, T. *Phys. Chem. Chem. Phys.* **2010**, *12*, 7748.
52. a) Ibrahim, M. A. *J. Comput. Chem.* **2011**, *32*, 2564; b) Jorgensen, W. L.; Schyman, P. *J. Chem. Theory Comput.* **2012**, DOI: 10.1021/ct300180w; c) Kolar, M.; Hobza, P. *J. Chem. Theory. Comput.* **2012**, *8*, 1325.
53. El Hage, K.; Piquemal, J.-P.; Hobaika, Z.; Maroun, R. G.; Gresh, N. *J. Comput. Chem.* **2013**, *34*, 1125.
54. a) Gourlaouen, C.; Piquemal, J.-P.; Parisel, O. *J. Chem. Phys.* **2006**, *124*, 174311; b) Gourlaouen, C.; Parisel, O. *Angew. Chem. Int. Ed.* **2007**, *46*, 553; c) van Severen, M.-C.; Piquemal, J.-P.; Parisel, O. *Chem. Phys. Letts.* **2009**, *478*, 17.
55. Devereux, M.; van Severen, M.-C.; Parisel, O.; Piquemal, J.-P.; Gresh, N. *J. Chem. Theory Comput.* **2011**, *7*, 138.
56. Tiraboschi, G.; Roques, B. P.; Gresh, N. *J. Comput. Chem.* **1999**, *20*, 1379.

57. Tiraboschi, G.; Gresh, N.; Giessner-Prettre, C.; Pedersen, L. G.; Deerfield, D. W. *J Comput Chem* **2000**, *21*, 1011.
58. Garmer, D. R.; Gresh, N.; Roques, B. P. *Proteins Structure, Function, and Genetics* **1998**, *31*, 42.
59. a) Gresh, N. *J. Phys. Chem. A* **1997**, *101*, 8690. b) Masella, M.; Gresh, N.; Flament, J. P. *J. Chem. Soc., Faraday Trans.* **1998**, *94*, 2745; c) Piquemal, J.-P.; Chelli, R.; Procacci, P.; Gresh, N. *J. Phys. Chem. A* **2007**, *111*, 8170.
60. Guo, H.; Gresh, N.; Roques, B. P.; Salahub, D. R. *J. Phys. Chem. B* **2000**, *104*, 9746.
61. Gresh, N.; Piquemal, J.-P.; Krauss, M. *J. Comput. Chem.*, **2005**, *26*, 1113.
62. Gresh, N.; Policar, C.; Giessner-Prettre, C. *J. Phys. Chem. A*, **2002**, *106*, 5660.
63. Ohrn, A.; Karlstrom, G. *J. Chem. Theory Comput.* **2007**, *3*, 1993.
64. Beachy, M. D.; Chasman, D.; Murphy, R. B.; Halgren, T. A. Friesner, R. A. *J. Am. Chem. Soc.* **1997**, *119*, 5908.
65. Gresh, N.; Kafafi, S. A.; Truchon, J.-F.; Salahub, D. R. *J. Comput. Chem.* **2004**, *25*, 823.
66. Rogalewicz, F.; Gresh, N.; Ohanessian, G. *J. Comput. Chem.* **2000**, *21*, 963.
67. Tiraboschi, G.; Fournie-Zaluski, M. C.; Roques, B. P.; Gresh, N. *J. Comput. Chem.* **2001**, *22*, 1038.
68. Gresh, N.; Shi, G.-B. *J. Comput. Chem.* **2004**, *25*, 160.
69. Faerman, C. H.; Price, S. L. *J. Am. Chem. Soc.* **1990**, *112*, 4915.

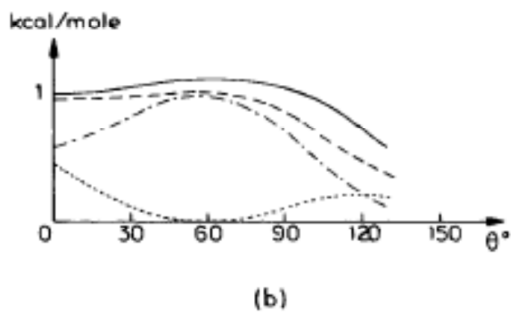
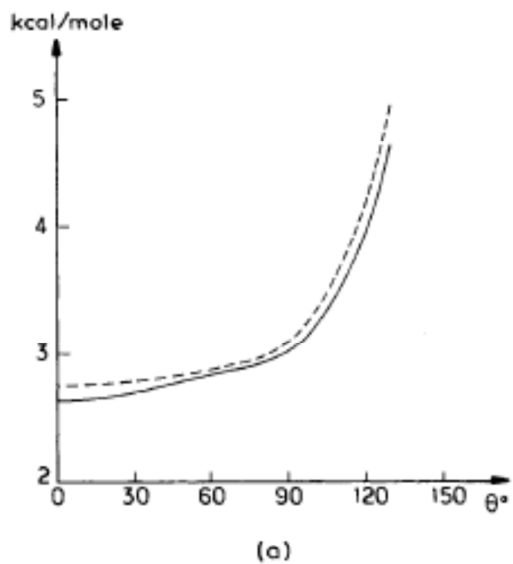
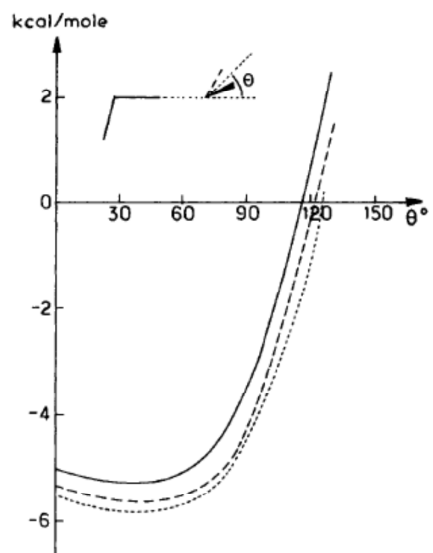
70. Chaudret, R.; Gresh, N.; Parisel, O.; Piquemal, J.-P. *J. Comput. Chem.* **2011**, *31*, 2949.
71. Barr, M. P.; Byrne, A. M.; Duffy, A. M.; Condron, C. M.; Devocelle, M.; Harriott, P.; Bouchier-Hayes, D. J.; Harmey, J. H. *Br. J. Cancer* **2005**, *92*, 328.
72. Borriello, L.; Montès, M.; Lepelletier, Y.; Leforban, B.; Liu, W.-Q.; Demange, L.; Delhomme, B.; Pavoni, S.; Jarray, R.; Boucher, J. L.; Dufour, S.; Hermine, O.; Garbay, C.; Hadj-Slimane, R.; Raynaud, F. *Cancer Lett.* **2014**, *349*, 120.
73. a) van der Kooi, C.; Jusino, M. A.; Perman, B.; Neau, D. B.; Bellamy, H. D.; Leahy, D. *Proc Natl Acad Sci USA* **2007**, *104*, 6152; b) Jarvis, A.; Allerston, C. K.; Jia, H.; Herzog, B.; Garza-Garcia, A.; Winfield, N.; Ellard, K.; Aqil, R.; Lynch, R.; Chapman, C.; Hartzoulakis, B.; Nally, J.; Stewart, M.; Cheng, L.; Menon, M.; Tickner, M.; Djordjevic, S.; Driscoll, P. C.; Zachary, I.; Selwood, D.L.; *J Med. Chem.* **2010**, *53*, 2215
74. Goldwasser, E.; de Courcy, B.; Demange, L.; Garbay, C.; Raynaud, F.; Hadj-Slimane, R.; Piquemal, J.-P.; Gresh, N. *J. Mod. Mol.* **2014**, *20*, 2472.
75. Silvi, B.; Savin, A. *Nature* **1994**, *371*, 683.
76. Piquemal, J-P, Pilme, J, Parise, I O, Gerard, H, Fourre, I, Berges, J.; Gourlaouen C, De La Lande A, Van Severen, M-C, Silvi, B. *Int J Quantum Chem* **2008**, *108*, 1951.
77. Evangelakis, G. A., Rizos, J. P., Lagaris, I. E., Demetropoulos, I. N. *Comput. Phys. Comm.* 1987, *46*, 401.
- 78 a) Zheng, J.; Yu, T.; Papajak, E.; Alecu, I. M.; Mielke, S.; Truhlar, D. G. *Phys Chem Chem Phys* **2011**, *13*, 10885; b) Tafipolsky, M.; Schmid R. *J. Comput Chem* **2005**, *26*, 1579.
79. a) Marchand, C. Maddali, K.; Metifiot, M.; Pommier, Y. *Curr. Top Med. Chem.* 2009, *9*, 1016; b) Klibanov, O. M. *Curr. Opin Invest. Drugs* **2009**, *10*, 190; c) Satom, M.; Motomura, T.; Aramaki, H.; Matsuda, T.; Yamashita, M.; Ito, Y.; Kawakami, H.; Matsuzaki, Y.; Watanabe, W.; Yamataka, K.; et al *J. Med. Chem.* **2006**, *49*, 1506; d) Schafer, J. J.; Squires, K. E. *Ann. Pharmacother.* **2010**, *44*, 145.

80. Hare, S.; Gupta, S.; Valkov, E.; Engelman, A.; Cherepanov, P. *Nature* **2010**, *464*, 232.
81. El Hage, K.; Piquemal, J.-P.; Hobaika, Z.; Maroun, R. G.; Gresh, N. *J. Comput. Chem* **2015**, *36*, 210.
82. El Hage, K.; Piquemal, J.-P.; Hobaika, Z.; Maroun, R. G.; Gresh, N. *J. Phys. Chem. A* **2014**, *118*, 9772.
83. Kitaura, K.; Morokuma, K. *Int. J. Quantum Chem.* **1976**, *10*, 325.
84. McCord, J.M., Fridovich, I. *J. Biol. Chem.* **1969**, *244*, 6049.
85. a) Somwar, R., Erdjumen-Bromage, H., Larsson, E., Shum, D, Lockwood, W. W., Yang, G., Sander, C., Ouerfelli, O., Tempst, P. J., Djaballah, H., Varmus, H. E. *Proc. Natl. Acad. Sci. U.S. A* **2011**, *108*, 16375; b) Glasauer, A., Sena, L. A., Diebold, L. P., A. P., Chandell N. S. *J Clin Invest.* **2014**, *124*, 117.
86. Bijere, L., Elias, B., Souhard, J.-P., Gicquel, E., Moucheon, C., Kirsch-de Mesmaeker, A., Vicendo, P. *Biochem.* **2006**, *45*, 6160.
- 87 .a) Hough, M. A., Hasnain, S. S. *Structure* **2003**, *11*, 937; b) Tainer J.A., Getzoff, E.D., Richardson, J.S. Richardson D.C. *Nature* **1983**, *306*, 284.
88. Gresh, N.; El Hage, K. E.; Perahia, D.; Piquemal, J.-P.; Berthomieu, C.; Berthomieu, D. *J. Comput Chem.* **2014**, *35*, 2096.
89. Lipparini, F., Lagardere, L., Stamm, B., Cances, E., Schnieders, M., Ren, P., Maday, Y., Piquemal, J.-P. *J. Chem. Theory Comput.* **2014**, *10*, 1638.
90. Krause, D.S.; Van Etten, R.A. *N. Engl. J. Med.* **2002**, *353*, S11.
91. a) Nikopoulos, S.; Giancotti, F. G. *Cell Cycle* **2005**, *4*, e131; b) McLean, G.W., Carragher, N.O., Avizienyte, V. G.; Frame, M. C. *Nature Cancer* **2005**, *5*, 505; c) Cohen, L. A.; Guan, J. L. *Curr. Cancer Drug Targers* **2005**, *5*, 629.
92. Lietha, D.; Cai, X.; Ceccarelli, D. F. J.; Li, Y.; Schaller, M. D.;Eck, M. *J. Cell* **2007**, *129*, 1177.

93. Choi, H. S.; et al. *Bioorg. Med. Chem. Lett.* **2006**, *16*, 2689.
94. de Courcy, B.; Piquemal, J.-P.; Garbay, C.; Gresh, N. *J. Am. Chem. Soc.* **2010**, *132*, 3312.
95. Langlet, J.; Claverie, P.; Caillet, J.; Pullman, A. *J. Phys. Chem.* **1998**, *92*, 1617.
96. Claverie, P.; Daudey, J.-P.; Langlet, J.; Pullman, B.; Piazzola, D., *J. Phys. Chem.* **1978**, *8*, 405.
97. a) Mundim, K. C.; Tsallis, C. *Int. J. Quantum Chem.* **1996**, *58*, 373; b) Moret, M. A.; Pascutti, P. G.; Bisch, P. M.; Mundim, K. C. *J Comput Chem* **1998**, *19*, 647.
98. Jiao, D.; Golubkov, P. A.; Darden, T. A.; Ren, P. *Proc. Natl. Acad. Sci. U.S.A.* **2008**, *105*, 6290.
99. Lietha, D.; Eck, M. J. *PLOS one*, **2008**, DOI: 10.1371/journal.pone.0003800.
100. Gracy, R. W.; Noltmann, E. A. *J Biol Chem* **1968**, *243*, 3161.
101. a) Patterson, J. H.; Waller, R. F.; Jeevarajah, D.; Billman-Jacobe, H.; McConville, M. J. *Biochem. J.* **2003**, *372*, 77; b) Garami, A.; Ilg, T. *J. Biol. Chem.* **2001**, *276*, 6566; c) Shinabarger, D.; Berry, A.; May, T. B.; Rothmel, R.; Fialho, A.; Chakrabarty, A. M. *J. Biol. Chem.* **1991**, *266*, 2080.
102. Roux, C.; Lee, J. H.; Jeffery, C. J.; Salmon, L. *Biochemistry* **2004**, *43*, 2926.
103. Cleasby, A.; Wonacott, A.; Skarzynski, T.; Hubbard, R. E.; Davies, G.; J.; Proudfoot, A. E. I.; Bernard, A. R.; Payton, M. A.; Wells, T. N. C. *Nat Struct Biol* **1996**, *3*, 470
104. Roux, C.; Gresh, N.; Perera, L.E; Piquemal, J.-P.; Salmon, L. *J. Comput. Chem.* **2007**, *28*, 938.
105. Gresh, N.; de Courcy, B.; Foret, J.; Courtiol-Legourd, S.; Piquemal, J.-P., Salmon, L. *J. Phys. Chem. B* **2011**, *115*, 8304.

- 106** a) Stevens, W. J., Basch, H., Krauss, M. *J. Chem. Phys.* **1984**, *81*, 6026; b) Stevens, W. J., Krauss, M., Basch, H.; Jasien, P. G. *Can. J. Chem.* **1992**, *70*, 612.
- 107.** a) Dunning, T. H. *J. Chem. Phys.* **1989**, *90*, 1007; b) Feller, D. *J. Comput. Chem.* **1996**, *17*, 1571.
- 108.** a) Law, M. M.; Hutson, J. M. *Comp. Phys. Comm.* **1997**, *102*, 252; b) Devereux, M.; Meuwly, M. *J. Chem. Inf. Model.*, **2010**, *50*, 349.
- 109.** Devereux, M.; Gresh, N.; Piquemal, J.-P.; Meuwly, M. *J. Comput. Chem.*, **2014**, *35*, 1577.
- 110.** Foster, J. M.; Boys, S. F. *Rev. Mod. Phys.* **1960**, *32*, 300.
- 111.** Chaudret, R; Gresh, N.; Cisneros, G. A.; Scemama, A.; Piquemal, J.-P. *Can. J. Chem.* **2013**, *91*: 1 dx.doi.org/10.1139/cjc-2012-0547.
- 112.** Piquemal, J.-P.; Cisneros, G. A.; Reinhardt, P.; Gresh, N.; Darden, T. A. *J. Chem. Phys.* **2006**, *124*, 104101.
- 113.** Chaudret, R.; Gresh, N.; Narth, C.; Lagardere, L.; Darden, T. A.; Cisneros, G. A.; Piquemal, J.-P. *J. Phys. Chem. A.* **2014**, *118*, 7598.
- 114.** C. Narth, L. Lagardère, E. Polack, N. Gresh, Q. Wang, J. W. Ponder, P. Ren, J.-P. Piquemal, *J. Chem. Theory. Comput.*, **2015**, submitted.
- 115** L. Lagardere, F. Lipparini, B. Stamm, E. Cancès, M. Schnieders, P. Y. Ren, Y. Maday, J.-P. Piquemal, *J. Chem. Theory. Comput.*, 2015, submitted.
- 116** F. Lipparini, L. Lagardere, B. Stamm, E. Cancès, M. Schnieders, P. Y. Ren, B. Mennucci, Y. Maday, J.-P. Piquemal, *J. Chem. Theory. Comput.* **2015**, online. DOI: [10.1021/ct500998q](https://doi.org/10.1021/ct500998q)
- 117.** a) Antony, J.; Gresh, N.; Olsen, L.; Hemmingsen, L.; Schofield, C. J.; Bauer, R. *J. Comput. Chem.*, **2002**, *23*, 1281; b) Antony, J., Piquemal, J.-P., Gresh, N. *J. Comput. Chem.*, **2005**, *26*, 1131.

- 118.** a) Gresh, N.; Derreumaux, P. *J. Phys. Chem. B* **2003**, *107*, 4862.; b) Miller Jenkins, L.M.; Hara, T.; Durell, S. R.; Hayashi, R.; Inman, J. K.; Piquemal, J.-P.; Gresh, N.; Appella, E. *J. Am. Chem. Soc.* **2007**, *129*, 11067.
- 119.** Gresh, N.; Audiffren, N.; Piquemal, J.-P.; de Ruyck, J.; Ledecq, M.; Wouters, J. *J. Phys. Chem. B* **2010**, *114*, 4884.
- 120.** Zhang, J.; Yang, W.; Piquemal, J.-P.; Ren, P. *J. Chem. Theory Comput.* **2012**, *8*, 1314.
- 121.** Nicolini, P.; Frezzato, D.; Gellini, C.; Bizzarri, M.; Chelli, R. *J. Comput. Chem.* **2013**, *34*, 1561.
- 122.** Marjolin, A.; Gourlaouen, C.; Clavaguéra, C.; Ren, P.; Wu, J.; Gresh, N.; Dognon, J.-P.; Piquemal, J.-P. *Theoret. Chem. Acc.*, **2012**, *131*, 1199.
- 123.** a) Muddana, H.; Gilson, M. K. *J. Chem. Theory Comput.* **2012**, *8*, 2023; b) Grimme, S. *Chem. Eur. J* **2012**, *18*, 9955.
- 124.** a) Gresh, N.; Sponer, J. *J. Phys. Chem. B.*, **1999**, *103*, 11415; b) Gresh, N.; Sponer, J. E.; Spackova, N.; Leszczynski, J.; Sponer, J. *J. Phys. Chem. B.* **2003**, *107*, 8669; c) Ghosh, D.; Kosenkov, D.; Vanovschi, V.; Williams, C. R.; Herbert, J. M.; Gordon, M. S.; Schmidt, M. W.; Slipchenko, L. V.; Krylov, A. *J. Phys. Chem. A* **2010**, *114*, 12739; d) Smith, Q. A.; Gordon, M. S.; Slipchenko, L. V. *J. Phys. Chem. A* **2011**, *115*, 11269; e) Savelyev, A.; MacKerell, A.D. *J. Comput. Chem.* **2014**, *16*, 1219.



Figures 1. Linear water dimer. Compared evolutions of a) $\Delta E(\text{SIBFA})$ and $\Delta E(\text{HF})$; b) E_{MTP} and $E_{\text{C}}(\text{HF})$; c) $E_{\text{ct}}(\text{SIBFA})$ and $E_{\text{ct}}(\text{HF})$.

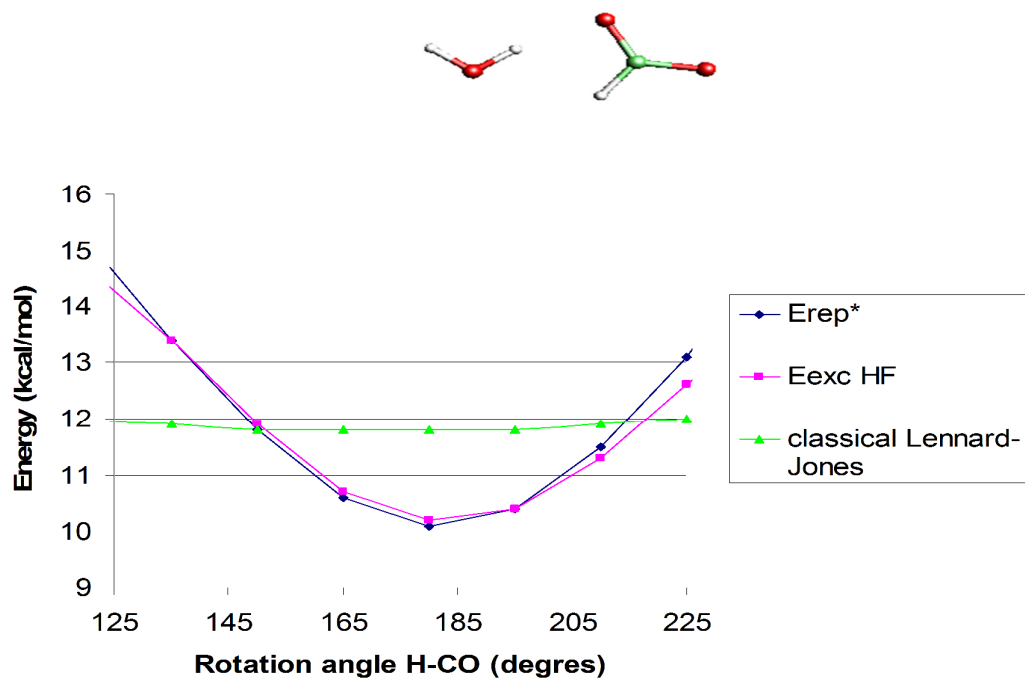
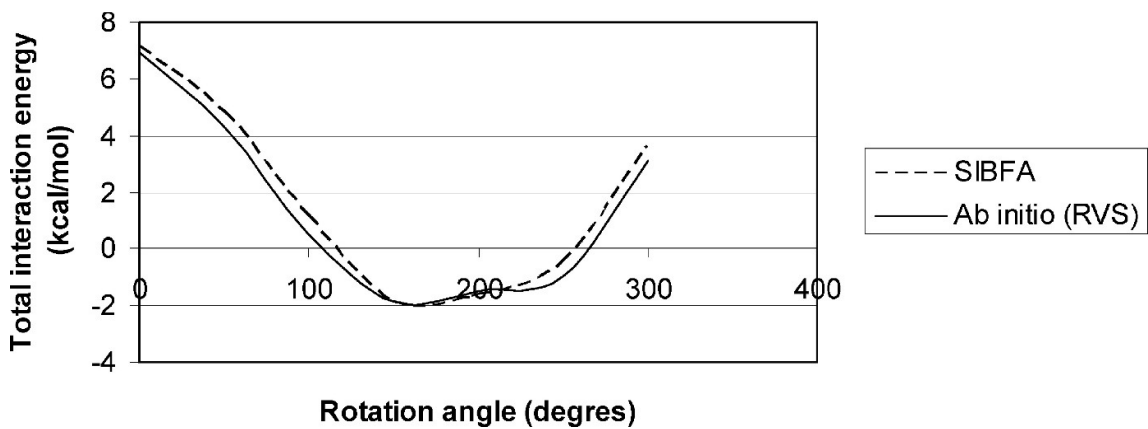
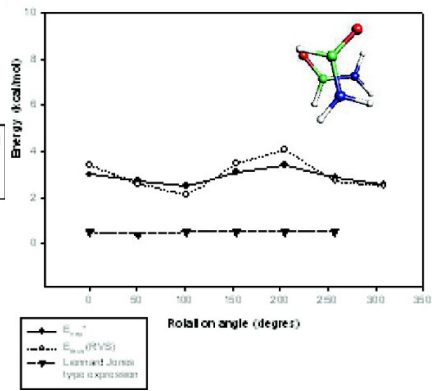
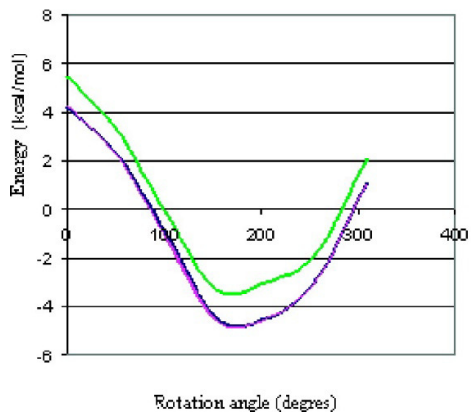
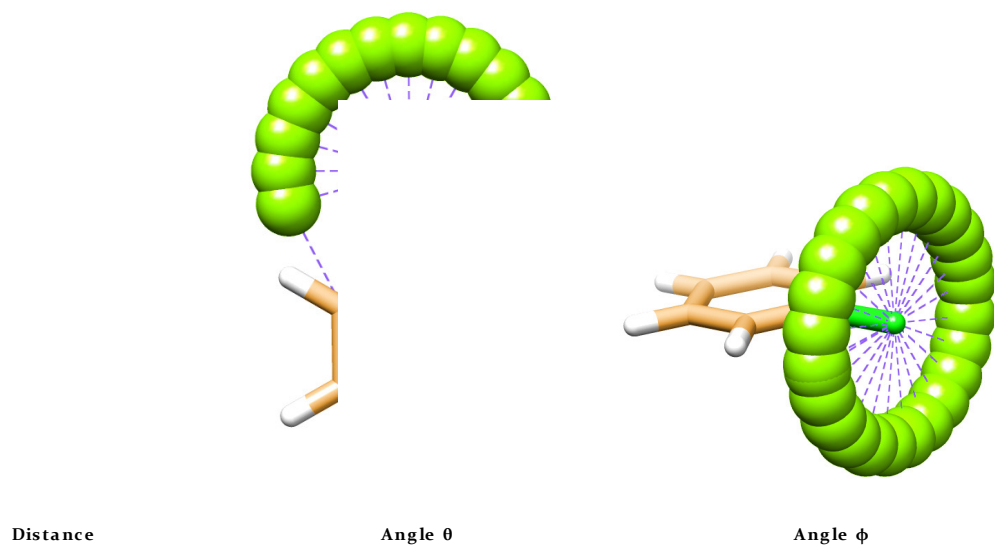


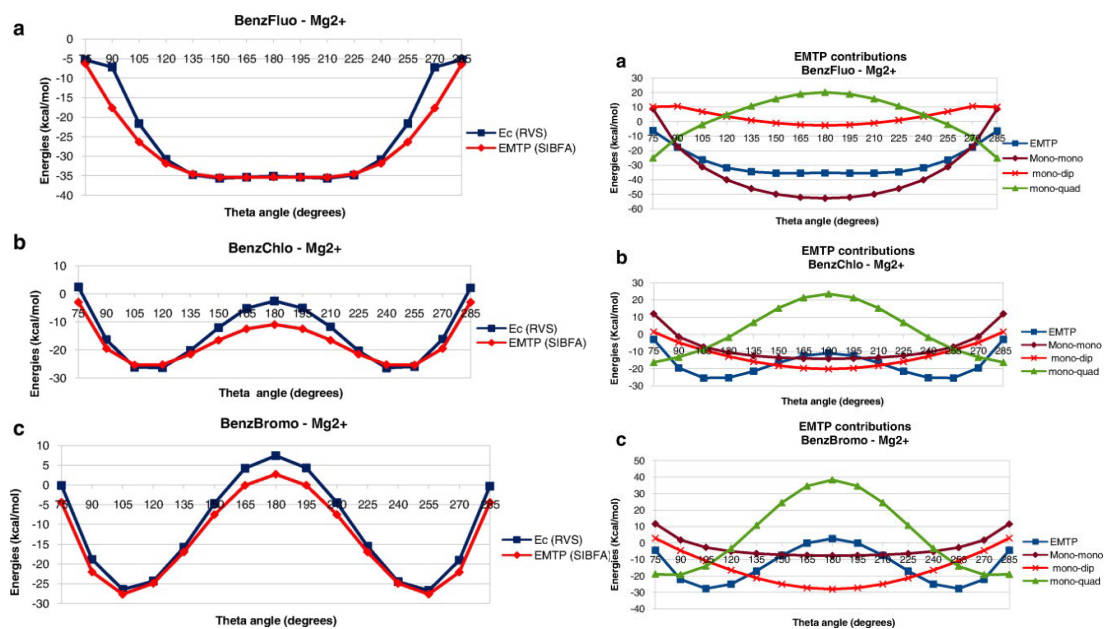
Figure 2. Monodentate formate-water. Compared evolutions as a function of the theta angle of $E_{\text{rep}}(\text{SIBFA})$, $E_{\text{exc}}(\text{HF})$, and a $1/R^{12}$ atom-atom repulsion.



Figures 3. Stacked formamide dimer. Compared evolutions of a) E_{MTP} and $E_C(HF)$; b) $E_{rep}(SIBFA)$ and $E_{exch}(HF)$; $\Delta E(SIBFA)$ and $\Delta E(HF)$.



Figures 4. Representation of the variations undergone by an Mg(II) probe around halobenzenes. a) in-plane variations of d with $\theta = 180^\circ$; b) in-plane variations of θ ; c) out-of-plane variations of ϕ .



Figures 5. a) Compared evolutions of E_C (HF) and E_{MTP} for in-plane variations of the theta angle for Mg(II) binding to the C-F, C-Mg, and C-Br bonds of halobenzene; b) in-plane theta evolutions of the charge-charge, charge-dipole, and charge-quadrupole components of E_{MTP} for Mg(II) binding to the C-F, C-Mg, and C-Br bonds of halobenzene.

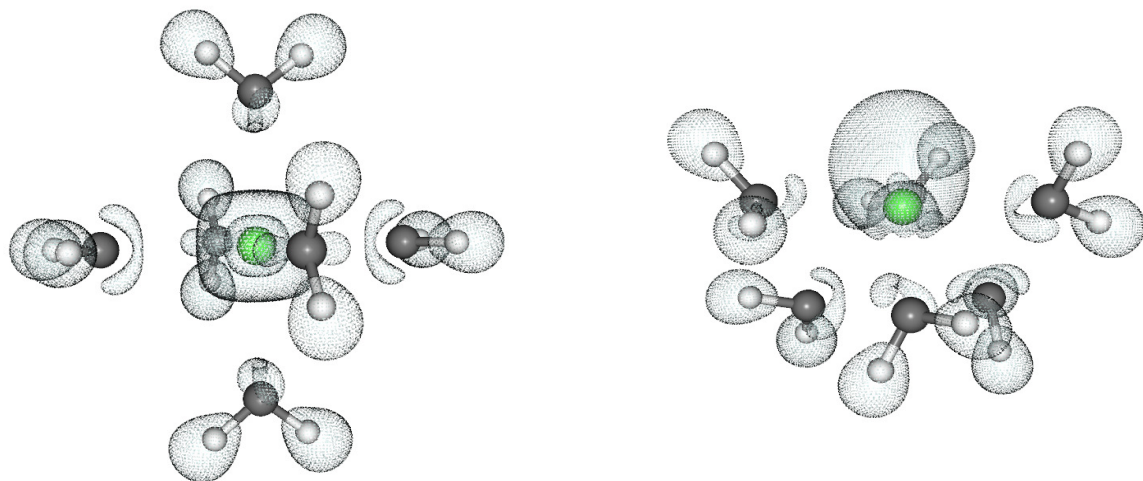


Figure 6. Representation of the tetraligated complex of Hg(II) with four water molecules in a) square planar and b) tetrahedral arrangements.

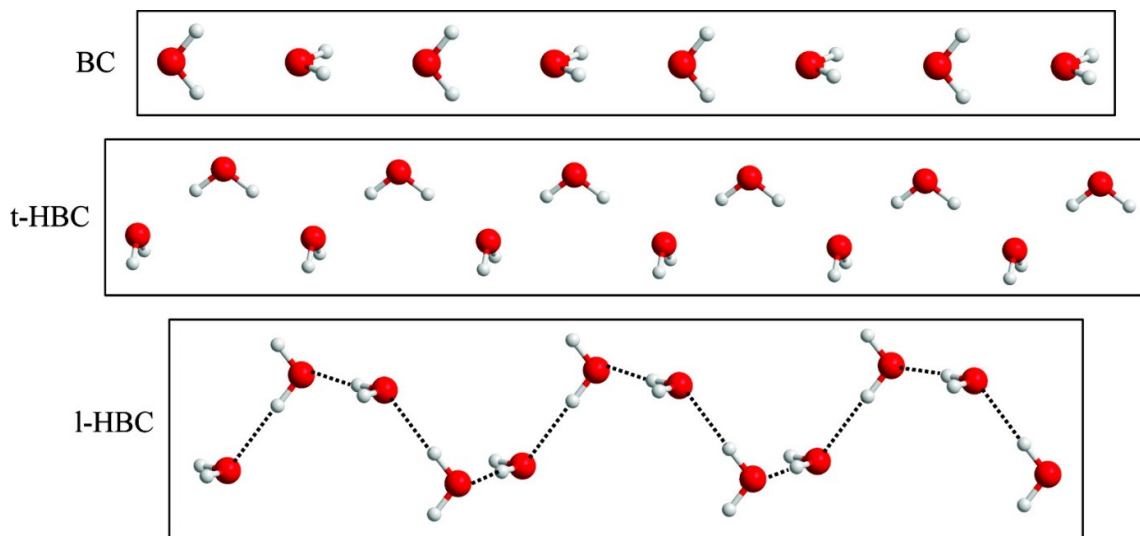


Figure 7. Representation of three water oligomers in transverse, bifurcated, and linear H-bonding arrangements.

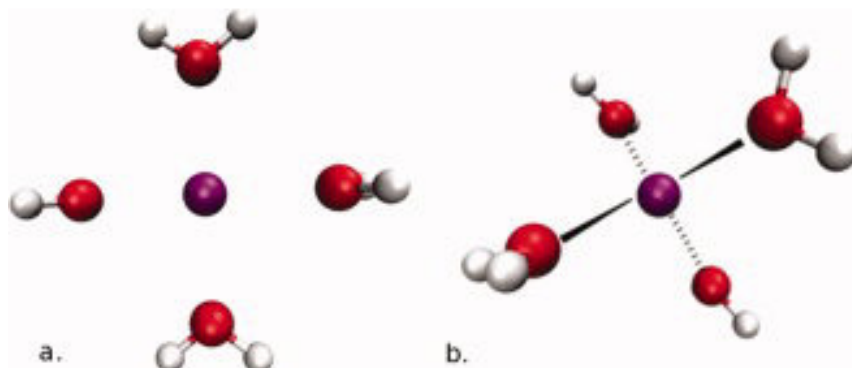
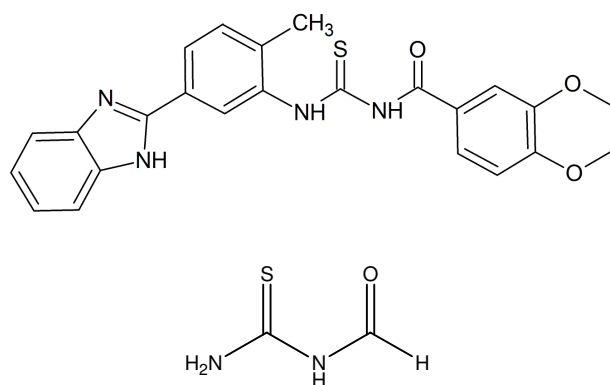


Figure 8. Representation of the $[\text{Hg}(\text{H}_2\text{O})_4]^{2+}$ complex in its a) square planar and b) tetrahedral arrangements.



Figures 9. Representation of a) the molecular structure of Lig-47 and b) of the structure of its central carboxythiourea (CTU) moiety.

Vol = 134.45 ua ³	Vol = 127.00 ua ³	Vol = 60.77 ua ³	Vol = 51.18 ua ³
Pop = 2.59 e ⁻	Pop = 2.77 e ⁻	Pop = 2.67 e ⁻	Pop = 2.77 e ⁻
r = 0.964 Å	r = 0.931 Å	r = 0.580 Å	r = 0.594 Å
θ = 106.6°	θ = 114.1°	θ = 116.9°	θ = 113.4°
φ = 3.5°	φ = -171.1°	φ = 1.5°	φ = -178.7°

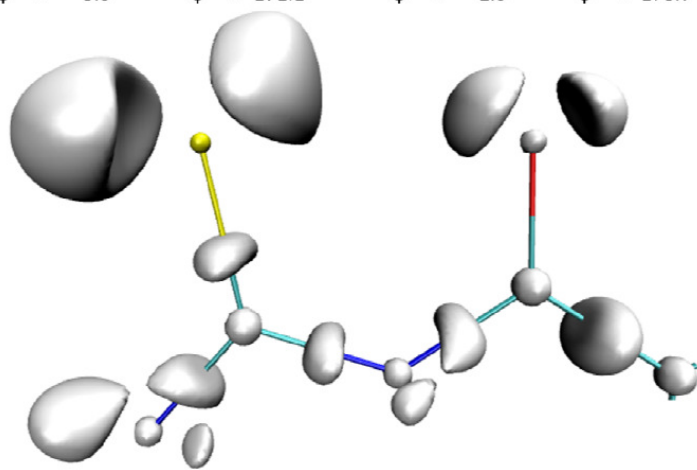


Figure 10. Representation of the ELF contours around the CTU locating the positions of the sp^2 lone-pairs of O and S atoms.

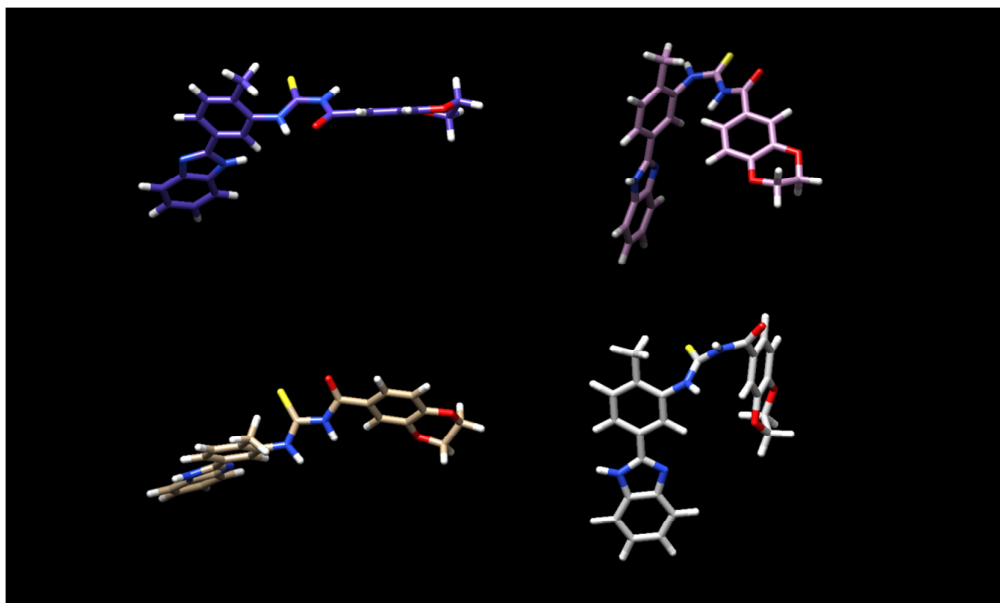


Figure 11. Three-dimensional structures of four representative energy-minimized conformations of Lig-47.

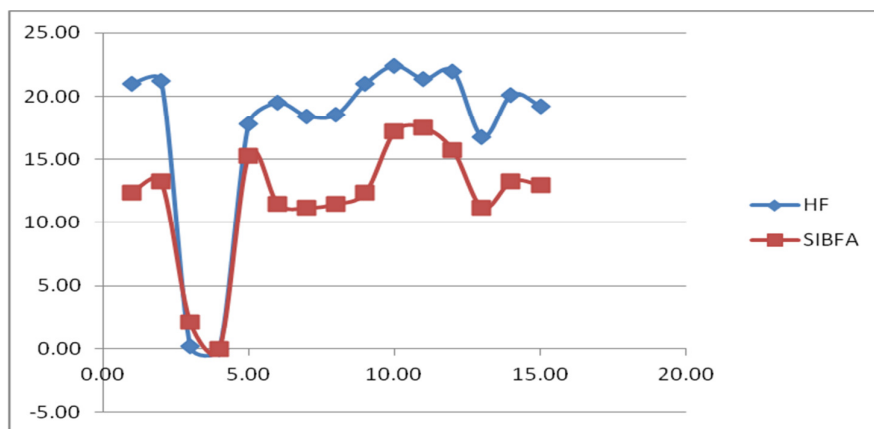
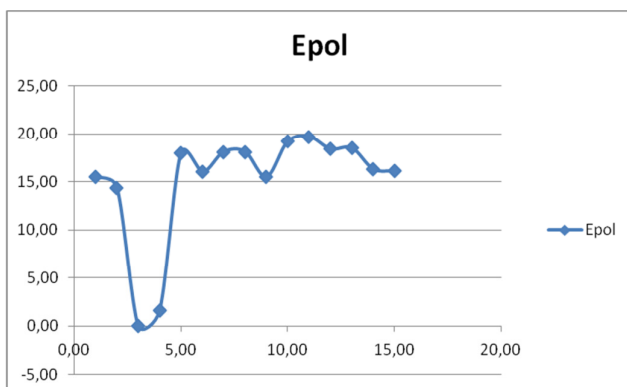
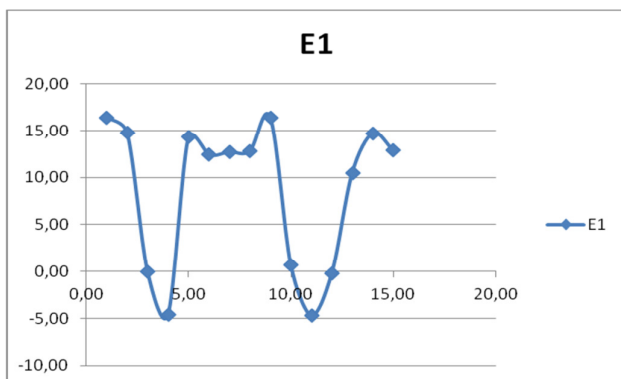
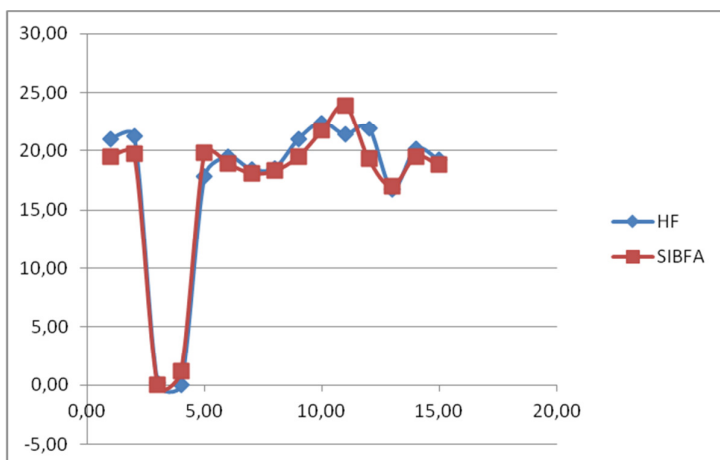
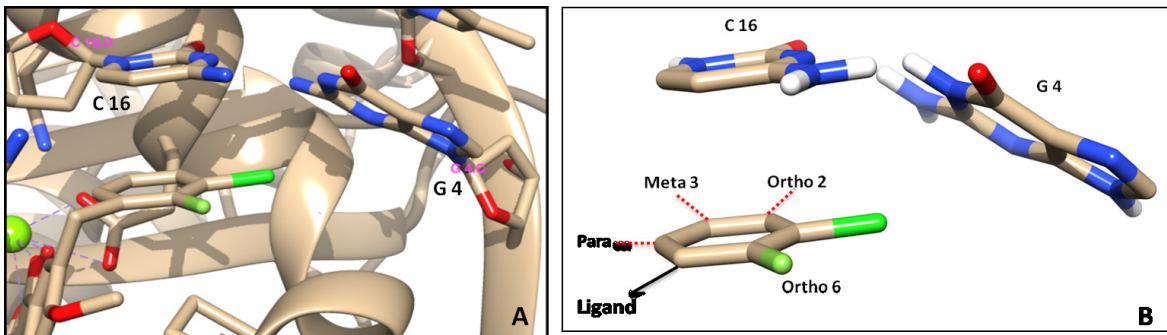
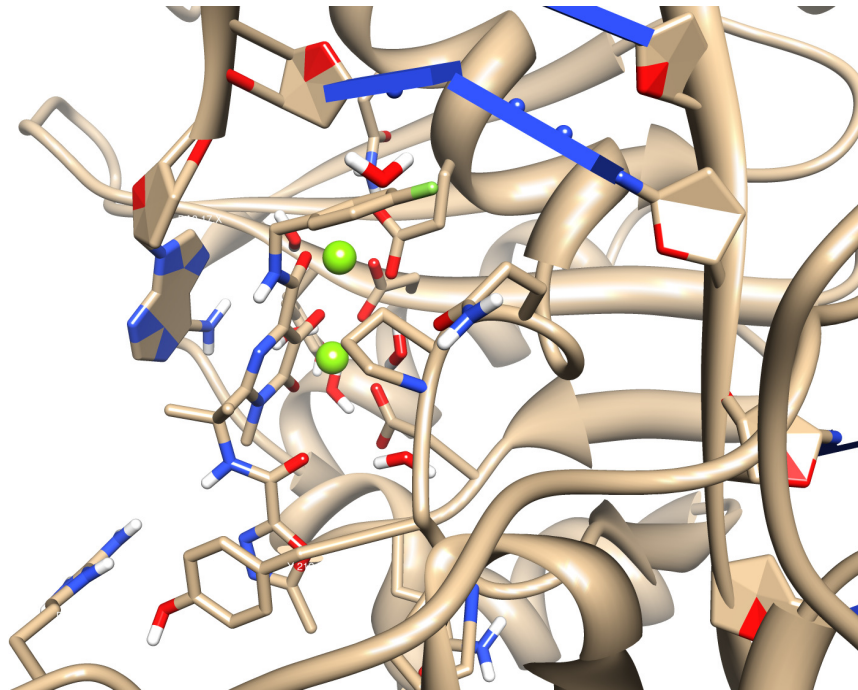


Figure 12. Compared evolutions of the relative QC/HF and SIBFA conformational energies as a function of the conformer number. Representation 'a' is used to construct CTU.



Figures 13. a) Compared evolutions of the relative QC/HF and SIBFA conformational energies as a function of the conformer number. Representation ‘b’ is used to construct CTU; b) corresponding evolutions of δE_1 ; c) corresponding evolutions of δE_{pol}



Figures 14. a) Representation of the three-dimensional structure of the Foamy virus integrase/DNA complex with elvitegravir; b) close-up on the interaction of the halobenzene ring with the G-C subsite.

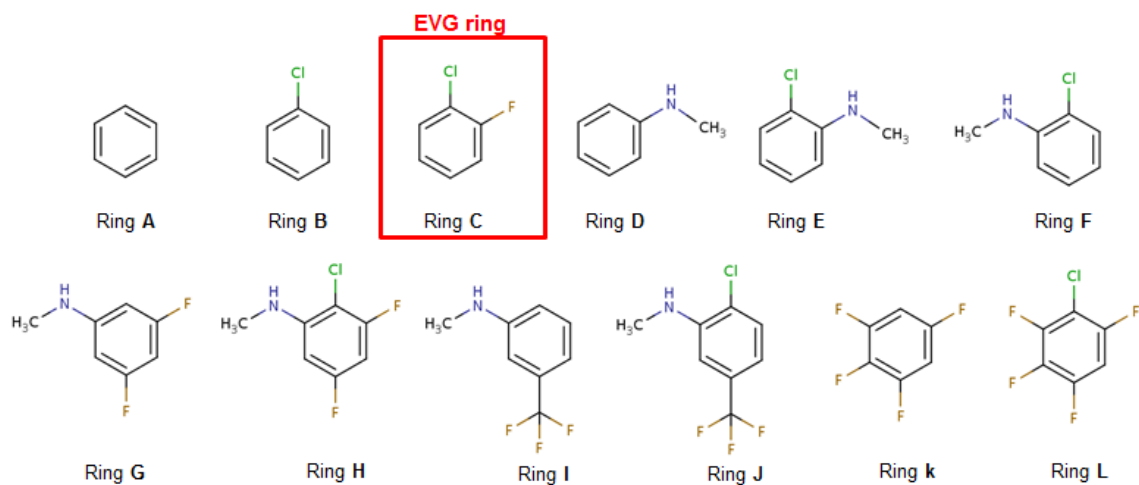
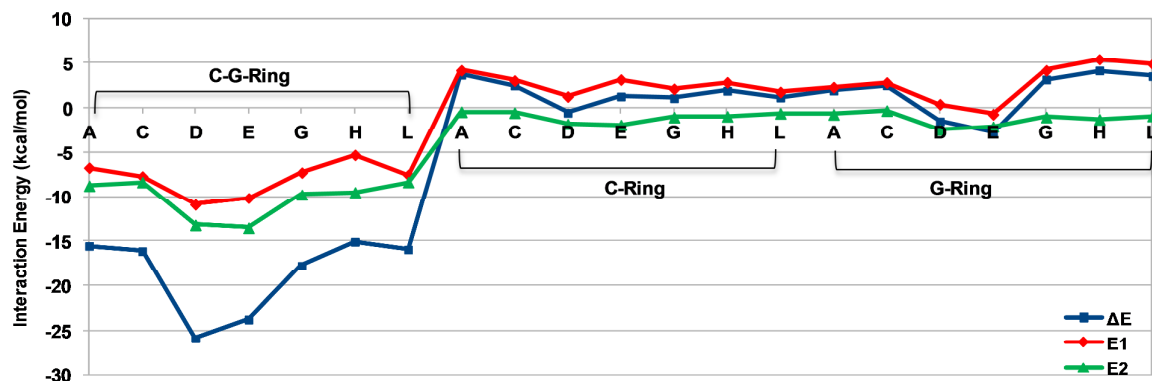
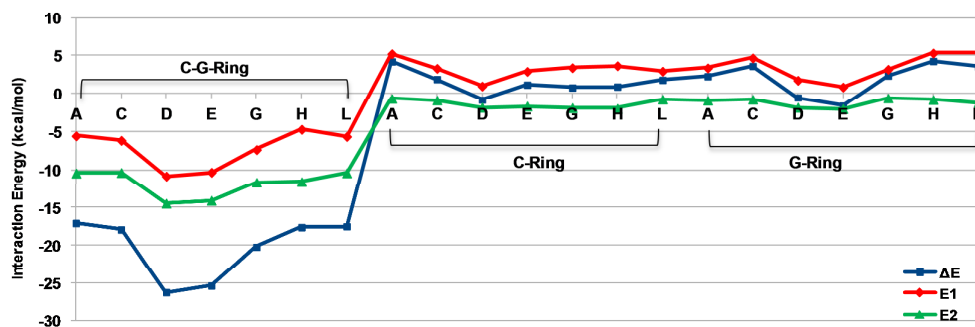


Figure 15. Molecular structures of halobenzene derivatives substituted with electron-donors or electron attractors, or with both.

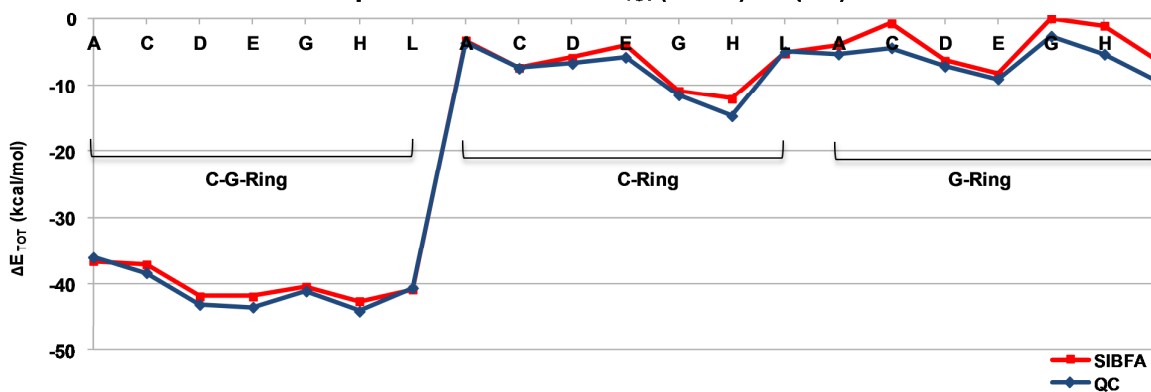
Evolution of E1 and E2 SIBFA



Evolution of E1 and E2 QC



Compared evolutions of ΔE_{TOT} (SIBFA) vs (QC)



Figures 16. a) Evolutions of the SIBFA E_1 , E_2 , and E_1+E_2 intermolecular interaction energies along a series of halobenzene derivatives; b) Evolutions of the QC E_1 , E_2 , and E_1+E_2 intermolecular interaction energies along a series of halobenzene derivatives; c) Compared evolutions of ΔE_{TOT} (SIBFA) and ΔE (DFT/QC) along a series of halobenzene derivatives.

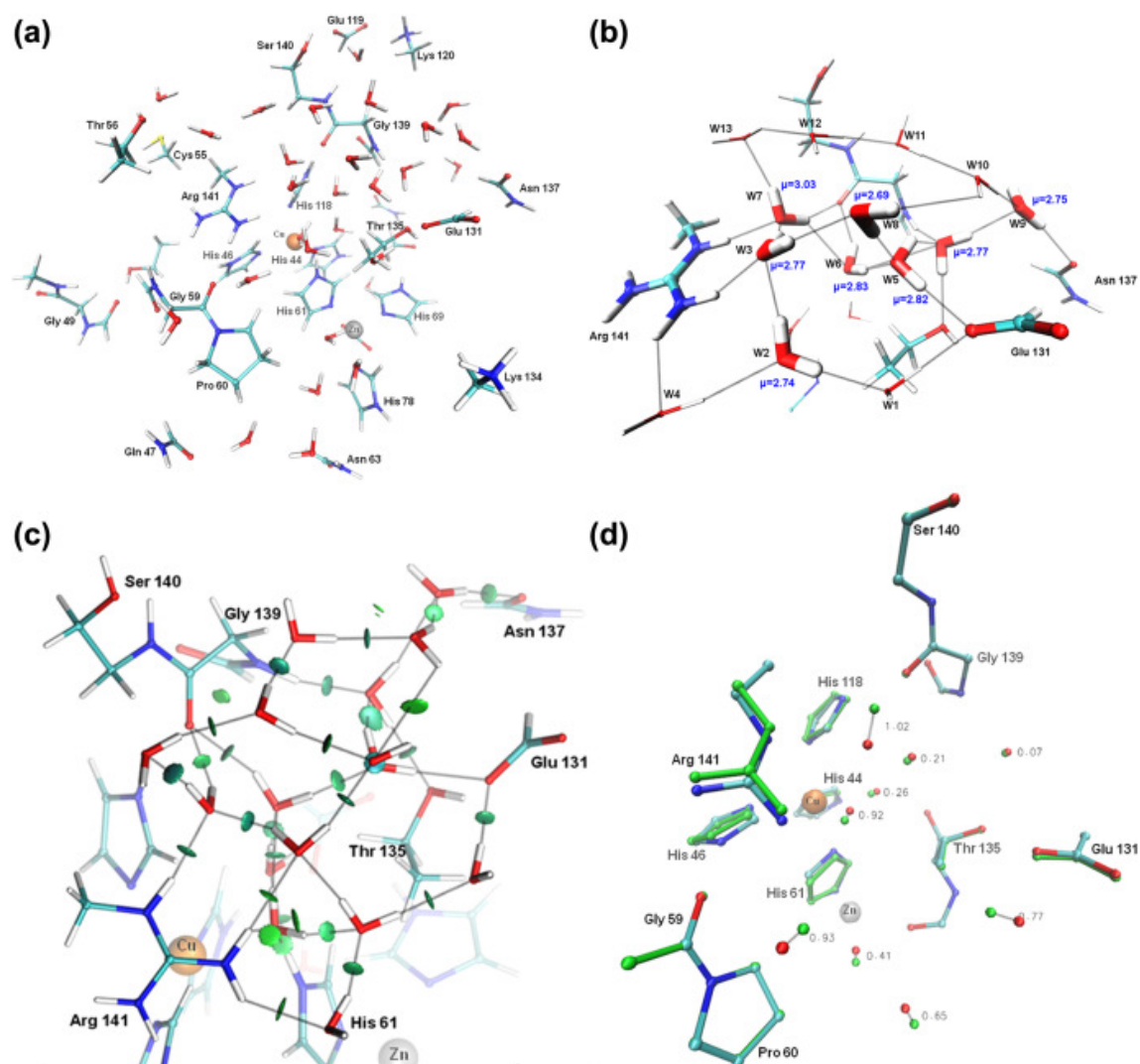


Figure 17. a) Organization of the most stable network of 28 waters around the bimetallic site of SOD; b) representation of the water networks and values of the highest dipole moments of structural waters.

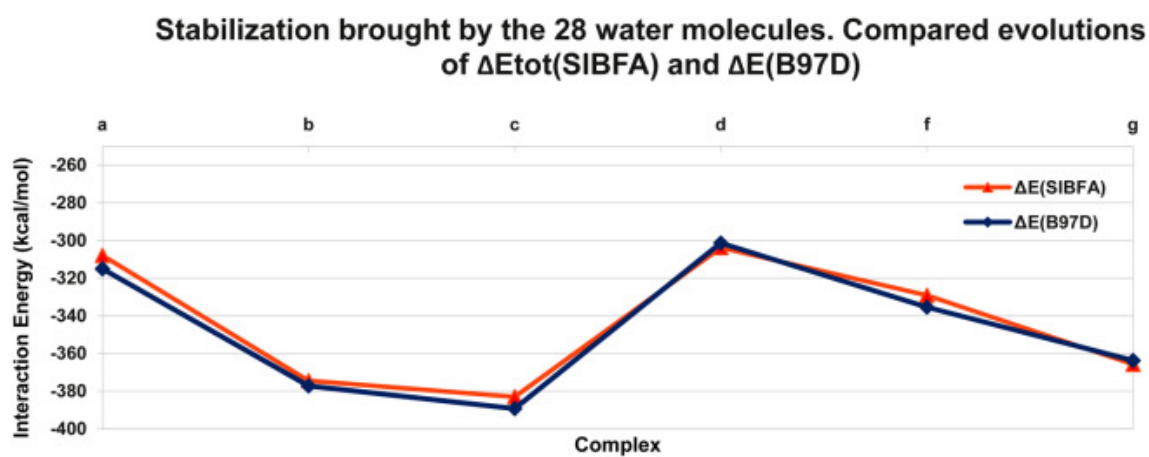
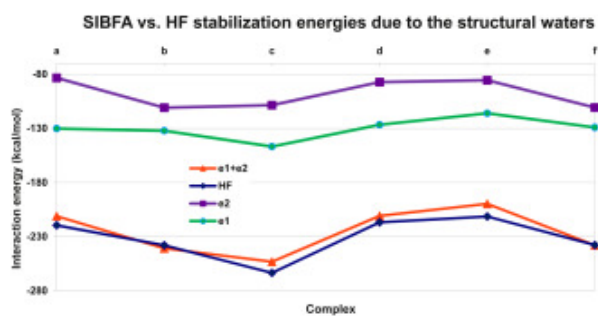


Figure 18. Stabilization brought by the 28-water networks in six distinct arrangements. A) Evolutions of $\Delta E(\text{QC})$ and of $\Delta E(\text{SIBFA})$ and its separate E_1 and E_2 terms. B) Evolutions of $\Delta E(\text{QC}/\text{B97D})$ and $\Delta E_{tot}(\text{SIBFA})$.

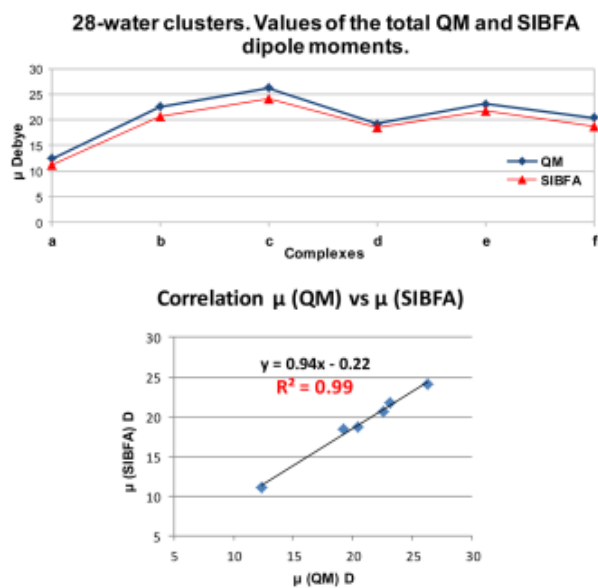
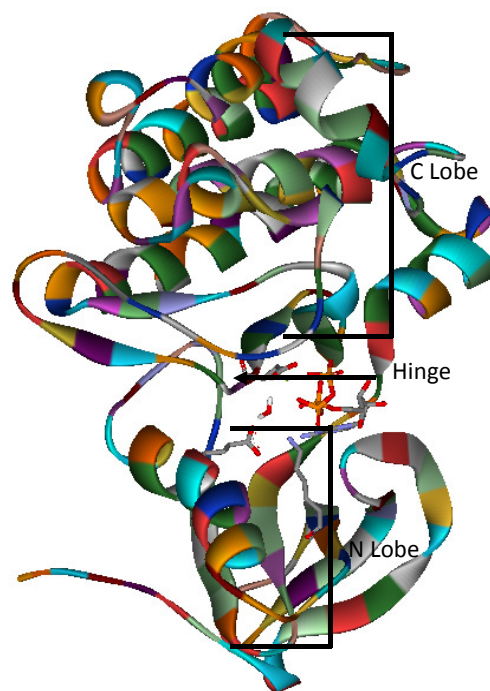


Figure 19. Compared variations of the QC and SIBFA values of the total dipole moments in six distinct 28-water networks.



Figures 20. Representation of the three-dimensional structure of FAK kinase.

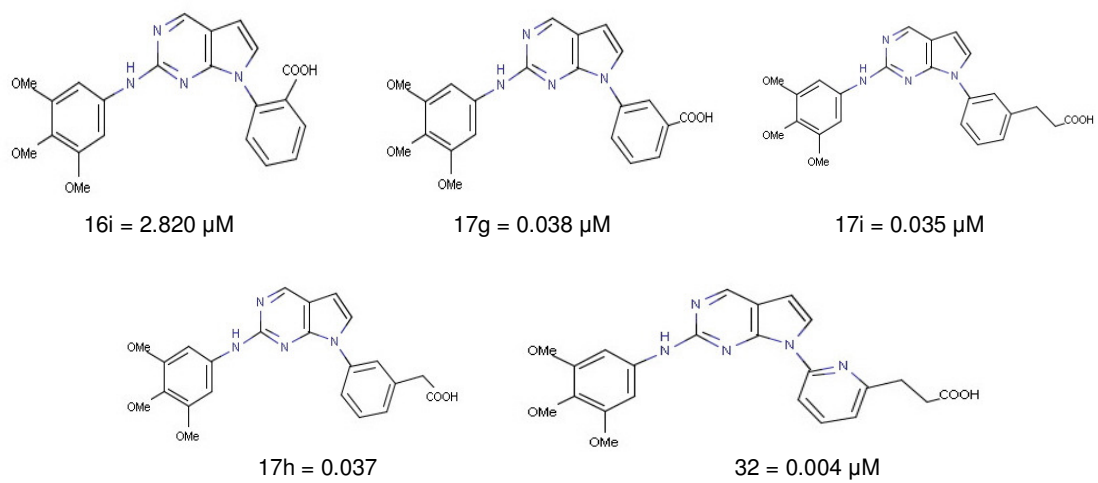


Figure 21. Representation of the molecular structures of the five pyrolopyrimidine inhibitors.

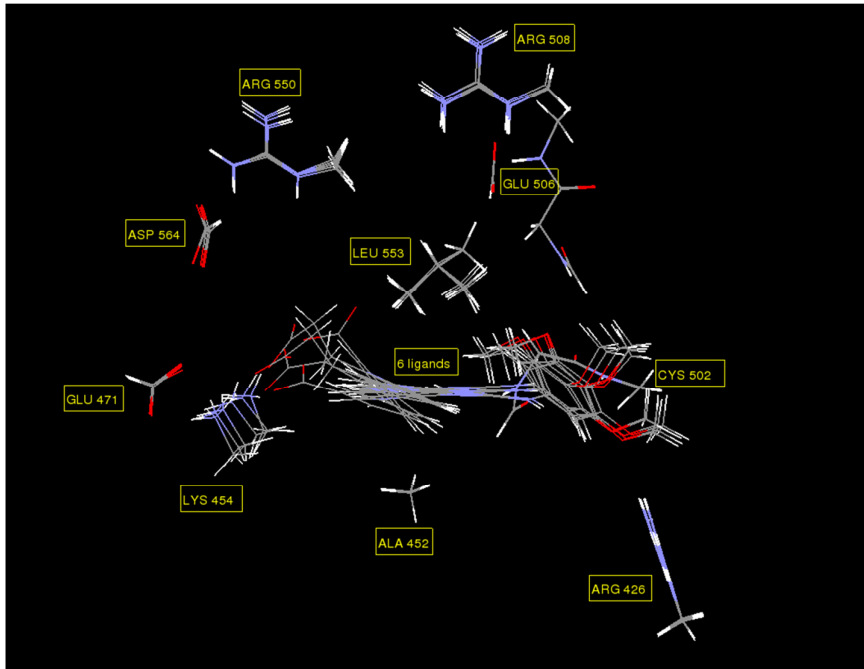


Figure 22. Overlay of the inhibitors in the FAK recognition site.

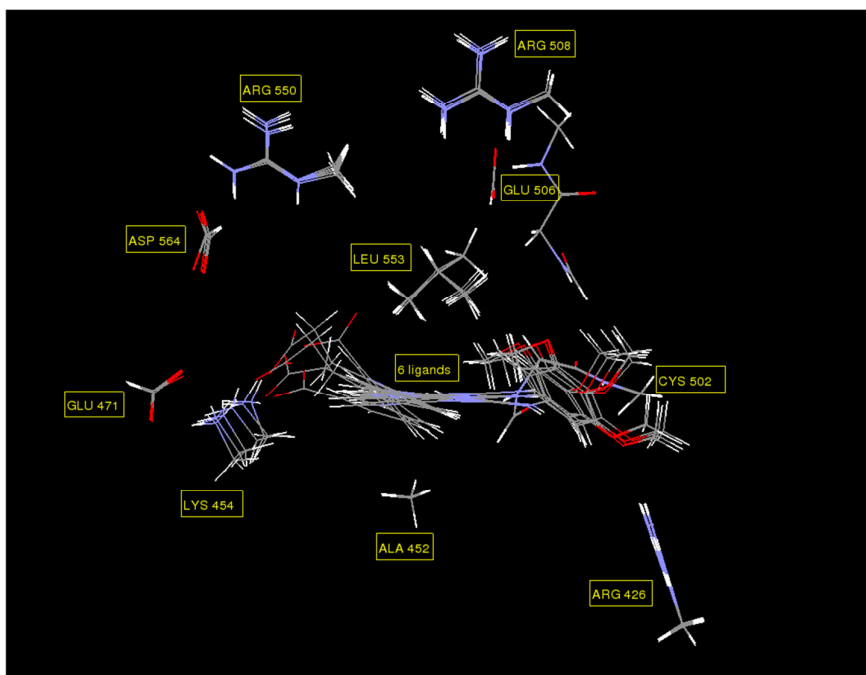


Figure 23. Representation of the complexes between the carboxylate group of the inhibitor and the ionic groups of the recognition site of FAK together with the discrete waters.

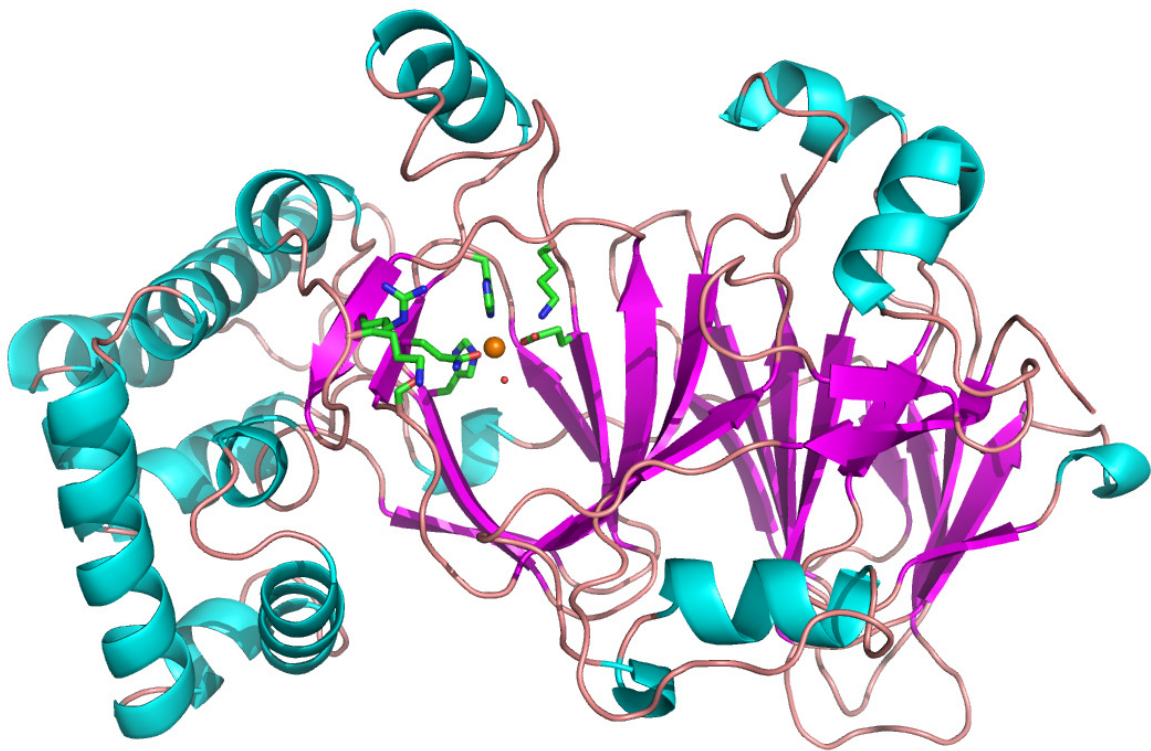


Figure 24. Three-dimensional structure of Zn(II)-bound PMI.

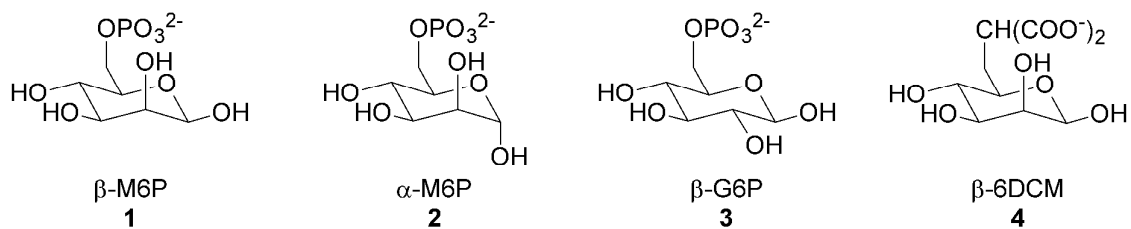


Figure 25. Representation of the structures of four PMI ligands

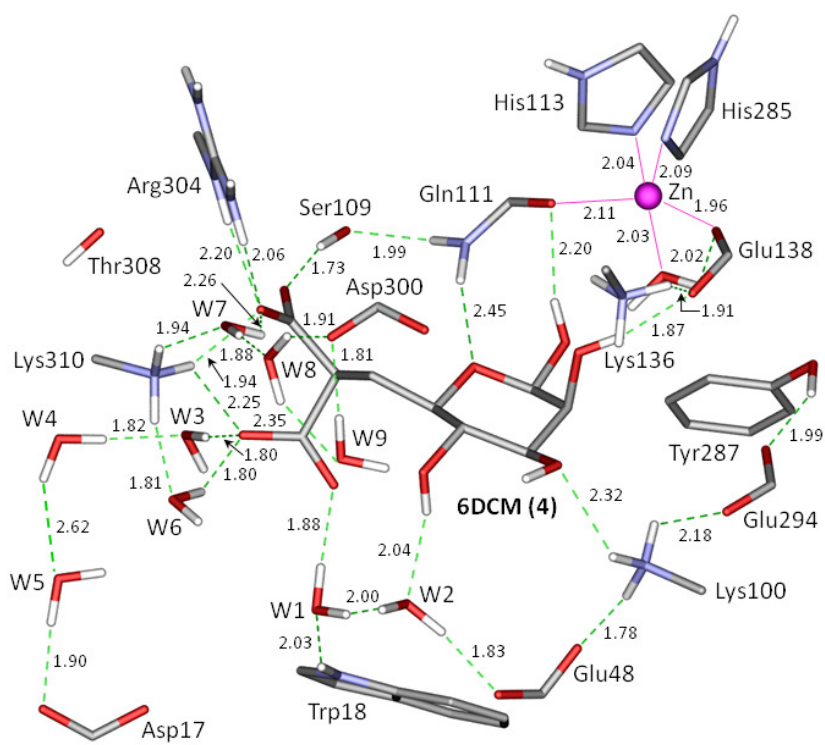


Figure 26. Representation of the optimized complex of the malonate derivative with PMI and nine water molecules.

	$[\text{Pb}(\text{H}_2\text{O})_4]^{2+}$				$[\text{Pb}(\text{H}_2\text{O})_5]^{2+}$				$[\text{Pb}(\text{H}_2\text{O})_6]^{2+}$			
	RVS		SIBFA		RVS		SIBFA		RVS		SIBFA	
	<i>hemi</i>	<i>holo</i>	<i>hemi</i>	<i>holo</i>	<i>hemi</i>	<i>holo</i>	<i>hemi</i>	<i>holo</i>	<i>hemi</i>	<i>holo</i>	<i>hemi</i>	<i>holo</i>
Coulomb (E_{mtp})	-179.	-171.	-181.	-172.	-206.	-198.	-210.	-201.	-229.	-224.	-235.	-229.
	7	4	1	8	4	8	0	9	0	3	9	2
repulsion (E_{rep})	103.5	87.5	103.1	85.1	106.1	91.9	106.9	91.1	108.2	94.5	111.8	95.3
pol. RVS (E_{pol}^*)	-70.2	-61.2	-64.9	-59.7	-71.2	-63.9	-67.6	-63.2	-70.4	-64.6	-67.7	-64.8
pol. VL (E_{pol})	-65.3	-54.2	-67.6	-55.0	-64.3	-54.5	-66.1	-56.1	-61.1	-53.1	-63.3	-55.9
Pb- polarization	-7.4	-1.6	-5.3	0.0	-6.1	-1.2	-4.5	-0.1	-6.0	-0.6	-4.7	0.0
charge- transfer (E_{ct})	-18.3	-15.8	-17.0	-16.4	-18.5	-16.3	-18.1	-17.5	-18.2	-16.7	-19.0	-18.2
total	-159.	-153.	-162.	-159.	-182.	-177.	-187.	-184.	-200.	-199.	-206.	-207.
	7	8	7	1	5	7	3	5	1	4	4	9

Table I. Polyligated complexes of Pb(II) with n=4-6 waters. Comparisons of the QC and SIBFA intermolecular interaction energies (in kcal/mol) and their contributions.

Table II. Polycordinated complex of Zn(II) with six water molecules. Values (kcal/mol) of the intermolecular interaction energies and of their individual contributions.

	$[\text{Zn}-(\text{H}_2\text{O})_6]^{2+}$		$[\text{Zn}-(\text{H}_2\text{O})_5-\text{H}_2\text{O}]^{2+}$		$[\text{Zn}-(\text{H}_2\text{O})_4-(\text{H}_2\text{O})_2]^{2+}$	
	RVS	SIBFA	RVS	SIBFA	RVS	SIBFA
E1	-209.1	-218.2	-191.9	-198.9	-174.8	-179.6
E _{pol}	-81.3	-78.9	-92.4	-89.5	-101.8	-99.3
E _{ct}	-20.6	-14.6	-24.5	-18.6	-28.7	-22.5
ΔE	-311.0	-311.7	-308.8	-307.0	-305.3	-301.4
E _{corr} /E _{disp}	-34.3	-35.9	-32.2	-35.3	-32.1	-37.3
ΔE_{tot}	-345.3	-347.7	-341.0	-342.3	-337.4	-338.7

Table II. Polyligated complexes of Zn(II) with 6 waters with 6, 5, and 4 first-shell waters. Comparisons of the QC and SIBFA intermolecular interaction energies (in kcal/mol) and their contributions.

$[\text{Hg}(\text{H}_2\text{O})_4]^{2+}$	Tetrahedral		Square planar	
	Ab initio	SIBFA	Ab initio	SIBFA
	E_{rep}	78.0	81.8	132.3
E_{c}	-194.2	-196.0	-226.9	-226.6
E_1	-116.1	-114.3	-94.6	-99.7
E_2	-89.3	-86.8	-101.7	-102.8
ΔE	-205.5	-201.1	-196.3	-202.5
$\Delta E_{\text{three-body}}$	1.7	1.6	4.8	4.8
$E_{\text{rep modified}}$	78.0	83.3	132.3	131.7
$\Delta E_{\text{modified}}$	-205.5	-199.6	-196.3	-197.7

Table III. Complexes of Hg(II) with four water molecules in square-planar and tetrahedral arrangements. Comparisons of the QC and SIBFA intermolecular interaction energies (in kcal/mol) and their contributions.

Non-additivity (kcal/mol)	ΔE		E_{POL}		E_{POL}^*	
	SIBFA	RVS	SIBFA	Morokuma	SIBFA	RVS
Ring A	0.3	0.1	0.2	0.3	0.3	0.3
Ring D	-1.1	-1.8	-1.2	-1.6	-0.7	-0.8
Ring E	-0.9	-1.3	-1.0	-1.2	-0.4	-0.5
Ring G	0.1	0.3	0.2	0.1	0.3	0.3
Ring H	0.7	0.6	0.4	0.4	0.4	0.6
Ring L	0.9	0.8	0.8	0.7	0.8	0.7

Table IV. Values of the binding non-additivities of a series of halobenzene derivatives for the G-C base pair of the HIV-1 binding subsite.

	16i	17g	17h	17g	32
E_1	35.6	22.5	-4.3	13.0	18.7
E_{pol}	-12.1	9.5	7.7	-6.5	-8.1
E_{ct}	-1.8	-1.2	-0.1	-1.4	-1.3
E_{disp}	-52.7	-48.8	-45.7	-51.2	-50.0
ΔE_{tot}	-30.9	-18.0	-42.3	-46.1	-40.7
ΔG_{solv}	14.8	4.8	22.4	25.8	24.8
$\Delta E_{\text{tot}} + \Delta G_{\text{solv}}$	-19.4	-17.5	-28.5	-22.0	-21.5
$\delta(\Delta E_{\text{tot}} + \Delta G_{\text{solv}})$	2.1	4.0	-7.0	-0.5	0.0

Table V. Relative energy balances for the binding of the five pyrrolopyrimidine inhibitors to FAK in the absence of the structural waters.

	E_{MTP} / E_C		E_{rep} / E_{exch}		E_1	
	SIBFA	RVS	SIBFA	RVS	SIBFA	RVS
16i	-206.0	-203.6	19.4	18.5	-186.6	-185.1
32	-194.0	-190.8	24.0	22.5	-169.9	-168.3
16i + 5 w	-348.1	-344.2	142.1	138.0	-206.0	-206.2
32 + 5 w	-352.4	-350.2	152.6	148.7	-199.8	-201.6

	E_{pol}		E_{ct}		$E_2 = E_{pol} + E_{ct}$	
	SIBFA	RVS	SIBFA	RVS	SIBFA	RVS
16i	-21.5	-23.3	-2.6	-2.6	-24.2	-25.9
32	-24.6	-26.7	-2.5	-3.0	-27.1	-29.7
16i + 5 w	-48.5	-51.3	-18.4	-16.6	-66.9	-67.9
32 + 5 w	-63.1	-66.0	-21.0	-19.6	-84.0	-85.6

	$\Delta E(SIBFA) / \Delta E(RVS)$	
	SIBFA	RVS
16i	-210.8	-210.0
32	-197.0	-196.9

Table VI. Energy decomposition for the binding of the carboxylate of the micro- and the nanomolar compounds to the ionic sites of FAK without and with the structural waters.

	16 i	17 g	17 h	17 g	32
E_i	47.1	34.3	57.8	60.3	61.4
E_{pol}	0.2	7.2	-14.4	-26.4	-28.6
E_{ct}	9.7	5.8	2.2	8.1	8.1
E_{disp}	-41.5	-49.8	-55.2	-53.5	-53.1
ΔE_{tot}	15.6	-2.5	-9.5	-11.6	-12.1
ΔG_{solv}	32.4	45.7	54.0	53.1	51.8
$\Delta E_{tot} + \Delta G_{solv}$	-1.8	-3.7	-6.1	-11.8	-14.1
$\delta(\Delta E_{tot} + \Delta G_{solv})$	12.3	10.3	8.0	2.3	0.0

Table VII. Relative energy balances for the binding of the five pyrrolopyrimidine inhibitors to FAK in the presence of the structural waters.

	a		b	
	1	4	1	4
E_{MTP}	-1453.8	-1437.0	-1272.8	-1223.8
E_{rep}	411.6	433.4	312.4	303.6
E_{l}	-1042.1	-1003.5	-960.4	-920.2
$\delta E_{\text{l}}(\mathbf{a-b})$	-81.7	-83.3		
E_{pol}	-176.0	-190.4	-152.1	-158.8
$\delta E_{\text{pol}}(\mathbf{a-b})$	-23.9	-31.6		
E_{ct}	-59.9	-68.3	-43.9	-47.1
$\delta E_{\text{ct}}(\mathbf{a-b})$	-16.0	-21.2		
$\Delta E(\text{SIBFA})$	-1278.1	-1262.2	-1156.4	-1126.1
$\delta E(\mathbf{a-b})$	-121.7	-136.1		
$\Delta E(\text{HF})^{\text{a}}$	-1268.2	-1243.0	-1145.2	-1104.3
$\delta E(\mathbf{a-b})^{\text{a}}$	-123.0	-138.7		
$\Delta E(\text{HF})^{\text{b}}$	-1278.9	-1253.1	-1148.9	-1107.3
$\delta E(\mathbf{a-b})^{\text{b}}$	-130.0	-145.8		
E_{disp}	-139.8	-138.7	-103.1	-97.4
$\Delta E_{\text{tot}}(\text{SIBFA})$	-1417.9	-1400.9	-1259.5	-1223.5

^a CEP 4-31G(2d) basis; ^b aug-cc-pVTZ(-f) basis.

Table VIII. Comparisons of the weights of the different energy contributions to the stabilization of the PMI-1 and PMI-4 complexes with and without the structural waters.